Influences of a Rough Bottom Topography on Flow Kinematics in an Eddy-Resolving Circulation Model

CLAUS W. BÖNING

Geophysical Fluid Dynamics Program, Princeton University, Princeton, New Jersey

(Manuscript received 15 September 1987, in final form 12 July 1988)

ABSTRACT

The effects of a rough topography are investigated in a primitive equation, eddy-resolving circulation model of an idealized ocean basin. The topography is chosen as a random field with an isotropic spectrum, specified according to observed abyssal hill topographies.

The interactions of the deep current fluctuations with the synoptic-scale irregularities of the ocean floor enhance the baroclinicity of the eddy field; whereas a strong tendency toward barotropization is revealed in a flat-bottom solution, the topographic influence leads to a substantial decrease of eddy kinetic energy below the thermocline and a much more depth-dependent structure, especially in areas of weaker flow intensity. Energy budgets indicate that the adjustment after the introduction of the bottom roughness is dominated by a strong reduction of energy in the external mode. While eddy energy in the thermocline is not significantly altered in the new equilibrium state, energy in the deeper layers is scrambled into smaller, topographic scales and effectively removed by lateral friction.

The velocity fluctuations in the thermocline exhibit a tendency toward phase-coherent vortices even in the interior, eastern portion of the gyre. Whereas eddies lose their identity after a few months in the flat bottom case, the presence of topography acts as a stabilizing factor; energetic, preferentially anticyclonic eddies show lifetimes of more than 1.5 years. The scale and propagation characteristics suggest a dynamical identification of these ringlike structures with the vortices of the "intermediate–geostrophic" (IG) regime.

Whereas the low-frequency variability in the flat bottom case is characterized by zonally oriented bands in the external mode, this structure disappears with the introduction of topography. A Lagrangian analysis shows that particle dispersion becomes almost isotropic below the thermocline; in the upper layers a preference of zonal diffusivity remains.

1. Introduction

Observational evidence suggests that mesoscale fluctuations dominate the flow field in nearly all parts of the world ocean. In the last decade, some progress has been made in understanding the evolution, equilibrium structure and dynamical significance of oceanic eddies. Observational and theoretical results are extensively summarized in Robinson (1983). Recently, a fine resolution, primitive equation model was used by Cox (1985, hereafter C85) to investigate the effect of eddies in the wind-driven and thermohaline circulation. The present study is intended to supplement the flat-bottomed model of C85 by introducing irregular depth variations in the interior of the model basin. The aim of the paper is to illuminate the influences of bottom roughness on the structure of the oceanic mesoscale variability in the context of a basin-scale circulation experiment.

The evolution and statistical equilibrium of mesoscale oceanic motions is controlled by a complex interaction of physical processes. Analytical as well as process-oriented numerical models have seeked to gain dynamical insight by studying various mechanisms in isolation. Comprehensive discussions of theoretical ideas and numerical results are given in the reviews of Rhines (1979), Haidvogel (1983), and Holloway (1986).

In a field of intense eddies, nonlinear processes are of particular importance. Nonlinearity can act in two completely different ways, depending on the scale (L) of the motions relative to the deformation radius (L_R) (Charney and Flierl 1981; Williams 1985). If isopycnal displacements are significant, as may be assumed for scales considerably larger than L_R, "intermediate–geostrophic" (IG) dynamics apply. Nonlinearity associated with density advection can effectively oppose the dispersion of energy by planetary waves and create a tendency to highly correlated, solitary vortices. For smaller scales, close to L_R, density advection can be neglected. In this "quasi-geostrophic" (QG) regime, nonlinearity associated with vorticity advection dominates and leads to highly interacting, turbulent eddy fields with energy cascading preferentially to both larger vertical and larger horizontal scales.

Corresponding author address: Institut für Meereskunde an der Universität Kiel, Düsternbrooker Weg 20, 2300 Kiel 1, FRG.

The energy decascade of quasi-geostrophic turbulence is eventually halted at horizontal scales where the variation of the Coriolis parameter with latitude becomes effective, and radiation of energy by planetary waves can redistribute energy in physical space. In a flat-bottomed, homogeneous ocean the competition between the turbulent behavior and wave dynamics was found to create a tendency to zonally elongated bands of barotropic flow (Rhines 1977). A structure of the low-frequency part of the fluctuations in accordance with the theoretical scenario was identified by Cox (1987, hereafter C87) in the interior of the flat-bottomed, eddy-resolving circulation model (C85).

Interactions of the flow field with irregularities of the bottom floor may constitute an important process that can inhibit the tendency towards barotropy and larger horizontal scales. Its effect depends on the scale of the fluid motion L relative to the topographic scale l and on the intensity of the flow (characterized by Ro $= U/fL$), relative to the strength of the relief (characterized by δ, the typical height variation divided by the mean ocean depth). In this paper we will be particularly concerned with the effect of the bottom variability on the scale of the energetic eddies, i.e., $L \sim l$.

If topographic variations are weak or the flow is strong, i.e. $\mathrm{Ro}/\delta \gg 1$, the flow dynamics will approach the limit of quasi-geostrophic turbulence. Topography has a stronger effect if the flow is weak and/or the height variability is large. An initially large-scale, slowly oscillating flow over severe roughness ($\mathrm{Ro} \ll \delta$) rapidly shrinks in scale (Rhines and Bretherton 1973). As energy is scattered into higher wavenumbers and vorticity variance is generated, a component of steady flow develops locked to the topography in the sense of anticyclonic circulation around hills (Holloway and Hendershott 1974; Bretherton and Haidvogel 1976). The flow scales decrease until $\mathrm{Ro}/\delta \sim 1$ and a balance is obtained between topographic effects and advective effects. The equilibrium energy spectrum becomes dependent on the topographic variance spectrum (Holloway 1978).

The influence of irregular topography on the vertical structure of eddies in a stratified ocean was investigated in quasi-geostrophic, periodic models of free-decaying turbulence by Rhines (1977). The results are critically reviewed and complemented by an investigation of the equilibrium case in a recent study of Treguier and Hua (1987). The main effect of topographic roughness found in these experiments is a stabilization of the baroclinic modes against the energy loss due to the nonlinear energy transfer into the barotropic mode. As a measure of the balance between the nonlinear and topographic effects, Rhines (1977) suggested the relevance of the ratio Ro/δ. The numerical experiments indicated a more baroclinic structure the smaller this parameter. Treguier and Hua (1987) point out that the effect of topography is better represented by the rms slope than by the rms height variation. A stronger rms slope tends to increase the surface intensification of eddy energy in the equilibrium solutions through a readjustment of the dynamics rather than through a direct intermodal energy transfer.

The idea that the structure of the eddy field in a given block of ocean, away from strong source regions, is locally determined according to the quasi-geostrophic scenario was elaborated by Owens and Bretherton (1978). The periodic, QG model successfully reproduced some basic statistical properties of the MODE eddies. All three processes, i.e., wave propagation, nonlinear interactions, and topographic interactions, were found to be important in determining the eddy structure in this region. Dickson (1983) reports an attempt to rationalize the greatly varying depth dependence of K_E as revealed by long-term current meter records in terms of the theoretical ideas outlined above. The resulting picture appears grossly consistent with the idea of a more depth-dependent eddy structure in weaker flow regimes and/or above severe topographic roughness and a less depth-dependent K_E in energetic regions and/or above smooth topography.

The role of eddies in the oceanic general circulation has been studied by means of fine resolution circulation models (Holland et al. 1983; Holland 1985). The numerical models have identified the release of mean field energy by baroclinic and/or barotropic instability processes as a major source of eddy variability, especially near the intense western boundary currents. The exploration of the sensitivity of flow statistics to various physical processes and changes in the external model parameters has mostly relied on the computationally more efficient QG models. Experiments mainly focus on the circulation in idealized model basins driven by steady wind fields. Careful comparisons of model results with observations of flow statistics in the western North Atlantic and North Pacific have been used to identify specific model problems (Schmitz and Holland 1982). The models seem to be capable now, by specific choices of parameters, to reproduce basic features of the distribution of mean flow and eddy statistics near the Kuroshio Extension and Gulf Stream reasonably well (Schmitz and Holland 1986). Schmitz and Holland (1982) reported one experiment in which an idealized, but variable bottom topography was introduced in the interior. The rather small-scale variability, with an rms deviation of 100 m from a mean depth of 5000 m, had no substantial influence on the energetic eddies and the mean flow structure in the jet region. Smaller abyssal energies, however, were found in the interior and seemed to be in better agreement with observations.

The applicability of quasi-geostrophic models of β-plane oceans to studies of the general circulation is limited, however. On larger scales, both the sphericity of the earth and geographical variations of the basic stratification cannot be neglected. In C85, the primitive equation model of Bryan (1969) was applied to an

idealized, but wide ocean basin to investigate the role of eddies in the thermohaline circulation. Except for an idealized coast and shelf along the western wall, the basin contained no topography. Eddies generated by baroclinic instability in the interior of the subtropical gyre were found to have a strong effect on distributions of conservative properties. Vast regions of rather uniform tracer and potential vorticity values characterized isopycnal surfaces in the subtropical thermocline.

The time dependence of the model flow was further analyzed by C87. As a particular feature, zonal barotropic bands ($\tau \sim 1.1$ years) dominated the low-frequency part of the spectrum. A Lagrangian analysis of the solution revealed a strong influence of the bands on particle trajectories. Single particle dispersion was strongly anisotropic, especially below the thermocline (Böning and Cox 1988). Indications of more low-frequency energy in zonal motions have been noted in some observational studies (Wunsch 1981; Richman et al. 1977); this behavior, however, seems to be confined primarily to the thermocline. A comparison of model particle behavior with observations of SOFAR-floats indicated that the anisotropy was much too strong in the deep model levels (Böning and Cox 1988).

In the present study the flat bottom case of C85 is supplemented by an experiment in which a variable bottom relief is introduced in the interior of the basin. In order to gain an understanding of the role the complex shape of the real ocean floor plays in the oceanic circulation, it seems useful to think of the topography as composed of two parts: a large scale, deterministic pattern represented by the configuration of the continental shelves, abyssal plains and midoceanic ridges, superimposed by a variety of smaller scale features of stochastic character. Several studies have been devoted to investigating the effect of large scale topographic contours on the oceanic general circulation (Holland 1973; Anderson and Killworth 1977). Recently, the influence of an idealized Mid-Atlantic Ridge on the eddy field and mean circulation (Verron et al. 1987) and on planetary wave processes generated by a fluctuating wind field (Barnier 1986) have been investigated with an eddy-resolving, QG model.

The focus of the present study is on the role of the smaller bathymetric scales which can be expected to exert a large, *direct* influence on the equilibrium structure of the fluctuating flow field, i.e., topographic roughness on scales comparable with the energetic mesoscale eddies. In order to separate these direct effects on the eddies from indirect effects due to altered mean flow dynamics, we try to avoid a topographic influence on the large-scale flow by not imposing topographic features with larger horizontal scales.

2. The numerical model

The experiment is based on the primitive equation, multilevel model of Bryan (1969) which in C85 was applied over an idealized basin of 60 degrees longitudinal width and extending from the equator to 65°N. The model is governed by the equations of motion and continuity

$$\frac{\partial \mathbf{v}}{\partial t} + \mathcal{L}\mathbf{v} + w\frac{\partial \mathbf{v}}{\partial z} + \mathbf{f} \times \mathbf{v} = -\frac{1}{\rho_0}\nabla p + K_m \frac{\partial^2 \mathbf{v}}{\partial z^2} + \mathbf{F}_m$$

$$\frac{\partial p}{\partial z} = -\rho g$$

$$\nabla \cdot \mathbf{v} + \frac{\partial w}{\partial z} = 0$$

and the conservation equation for density

$$\frac{\partial \rho}{\partial t} + \mathcal{L}\rho + w\rho_z = \frac{K_d}{\gamma}\frac{\partial^2 \rho}{\partial z^2} + \mathbf{F}_d$$

which is a linear function of the single state variable T. The ∇ operator and the nonlinear advection operator $\mathcal{L}$ apply to horizontal variations only; K_m ($=10$ cm^2 s^{-1}) and K_d ($=0.3$ cm^2 s^{-1}) are the vertical mixing coefficients corresponding to m: momentum, d: density. Lateral mixing is given in biharmonic form, $\mathbf{F}_m = -A_m\nabla^4\mathbf{v}$, and $F_d = -A_d\nabla^4\rho$, with $A_m = 8 \times 10^{18}$ cm^4 s^{-1}, $A_d = 2.4 \times 10^{19}$ cm^4 s^{-1}. In the case of a statically unstable stratification, a "convective mixing" of density occurs through the delta function,

$$\gamma = \begin{cases} 1, & \text{if } \partial\rho/\partial z \geq 0 \\ 0, & \text{if } \partial\rho/\partial z < 0. \end{cases}$$

The flow is driven by a steady zonal wind stress τ^w and by a relaxation of the surface temperature towards prescribed reference values, which are linearly decreasing with latitude. At the bottom, a quadratic drag law is used,

$$\tau^b = \rho_0 c_0 (u^2 + v^2)^{1/2}(u\cos\alpha - v\cos\alpha, \quad u\sin\alpha + v\cos\alpha),$$

$$c_0 = 1.3 \times 10^{-3}, \quad \alpha = 10°.$$

In C85, a model basin with a flat bottom was used, except for an idealized coast and shelf along the western wall. In the present study an irregular topography is introduced in the interior of the domain. Since it is not the intention here to simulate an actual ocean basin, but to apply an idealized bathymetry with reasonable "roughness" at the scales of the energetic eddies, a random, isotropic topography is used. A $K^{-1.5}$ variance spectrum is chosen similar to the observed spectrum of Bell (1975) who found characteristic slopes close to K^{-2}, except for a flattening at the lower wavenumbers in abyssal plains (Fig. 1).

The irregular topography is introduced in the interior of the basin (Fig. 2). No changes relative to the flat bottom case of C85 have been made with respect to the shelf configuration along the western wall in order

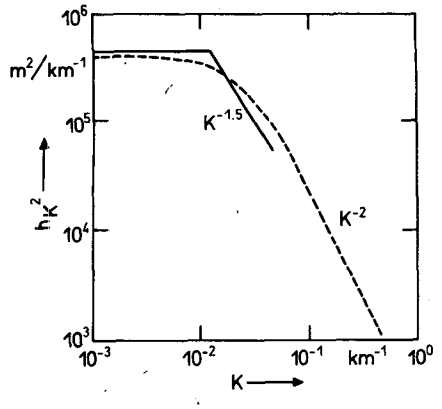

FIG. 1. Scalar wavenumber spectrum of the model topography in the interior of the basin (full line). The dashed line indicates an observed spectrum of abyssal hill topography (adapted from Bell 1975).

to avoid direct topographic influences on the boundary current (which, in turn, could drastically alter the flow field in the interior).

The grid size of the model is ⅓° in meridional, and 0.4° in zonal direction which gives an equal spacing of $\Delta = 37$ km at 33° latitude. This corresponds to a highest wavenumber $K_s = 8.5 \times 10^{-2}$ km^{-1}, which is resolved by the grid. In order to allow the representation of the topography and the topographically induced small flow scales on the numerical grid, the model spectrum (Fig. 1) is truncated at wavenumber $K_s/2$; i.e., the smallest topographic features have wavelengths of 4Δ. Larger topographic scales are de-emphasized, by prescribing a white spectrum for $K < K_s/7$.

The truncation of the topographic spectrum, together with the strongly scale-selective damping, prevents an intensification of motion with scales near the grid resolution. Since, according to linear theory, high vertical shear above topography is only expected for flow scales small compared with the radius of deformation, the vertical grid size appears to be less constrained by the flow scale than by an adequate representation of the depth variations. To obtain sufficient resolution, the number of vertical grid boxes have been increased from 18 used in C85 to 21 in the present study. Figure 3 indicates the vertical distribution of the grid boxes for both cases. The mean depth H of the model basin is 3650 m (4000 m in C85). With a rms-height deviation h of 400 m, the roughness parameter δ is of o(0.1).

In C85, the fine resolution, flat bottom model was run for 24 years, after a basic stratification and circulation was allowed to build up during 540 years of integration on a coarser (1°), noneddy resolving grid. Due to the reduced model friction on the fine grid, the solution readily became energetic with mesoscale fluctuations. The pattern of eddy kinetic energy in the main thermocline did not change substantially between the intervals of years 12 to 18, and 18 to 24, respectively, indicating that the upper ocean had reached a new adjustment within this integration period.

The present model with bottom topography was initialized at year 16 of C85 and integrated for 11 years

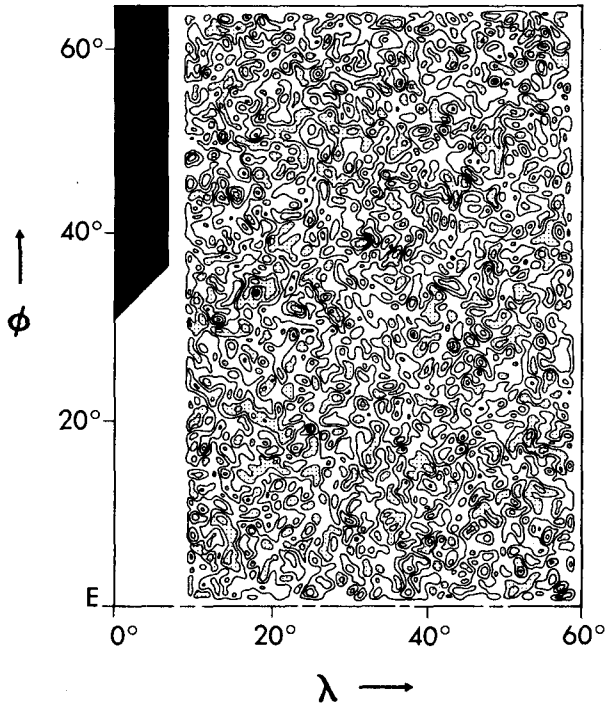

FIG. 2. The model basin with the bathymetry in the interior. The contour interval is 300 m. (The shelf along the western wall is not shown.)

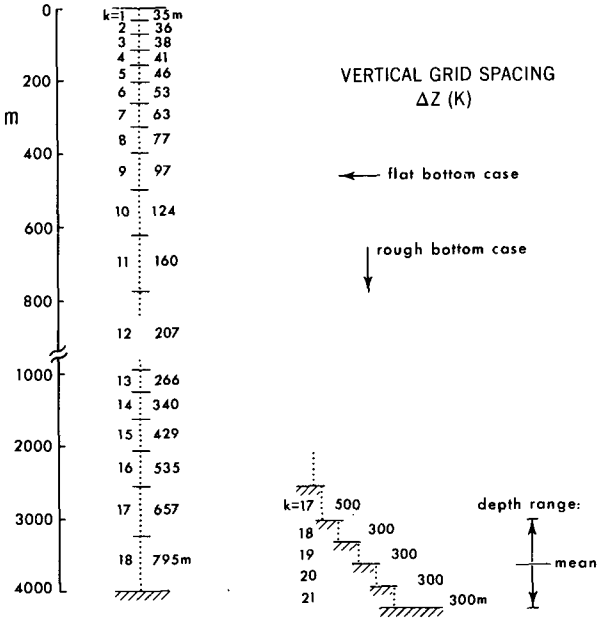

FIG. 3. Vertical grid boxes in the rough bottom experiment compared to the flat bottom case of Cox (1985).

which appeared to be sufficient for the eddy field to adjust to the new conditions. As in the flat bottom case, the integration period is clearly not long enough for the large-scale aspects of the deep ocean circulation to respond to the altered dynamics and to reach a new equilibrium. The discussion of the model solution will focus on the kinematical properties of the eddy field in the rough bottom case relative to the flat bottom solution.

3. Energetic adjustment

Information about the energy cycle of the model system may be obtained from the work terms which determine the kinetic energy of the flow. Using the notation

$\langle\ \rangle$ volume average

$[\ ]$ horizontal space average

$\bar{}$ vertical average

$\hat{}$ vertical deviation

the time-rate-of-change of the total kinetic energy of the ocean basin is given by

$$K_t = W + B + \mathrm{LF} + \mathrm{BD} + \mathrm{IF}$$

where

$$W = [\mathbf{v}\cdot\boldsymbol{\tau}^w]$$

is the work of the wind stress $\boldsymbol{\tau}^w$ at the surface

$$B = -\langle g\rho w\rangle$$

is the work by buoyancy forces in the interior, representing a conversion of potential energy to (or from) kinetic energy, and

$$\mathrm{LF} = -\rho_0 A_m\langle \mathbf{v}\cdot\nabla^4\mathbf{v}\rangle$$

$$\mathrm{BD} = -[\mathbf{v}\cdot\boldsymbol{\tau}^b]$$

$$\mathrm{IF} = -\rho_0 K_m\langle \mathbf{v}_z\cdot\mathbf{v}_z\rangle$$

give the work of tangential stresses at the walls, at the bottom, and the dissipation in the interior of the fluid, respectively.

If the kinetic energy per unit volume K is divided into the external and internal components,

$$\bar{K} = \langle \rho_0(\bar{\mathbf{v}}\cdot\bar{\mathbf{v}})/2\rangle$$

$$\hat{K} = \langle \rho_0(\hat{\mathbf{v}}\cdot\hat{\mathbf{v}})/2\rangle$$

one can show that (e.g., Holland 1975)

$$\bar{K}_t = W_e + B_e + N_e + \mathrm{LF}_e + \mathrm{BD}_e$$

$$\hat{K}_t = W_i + B_i + N_i + \mathrm{LF}_i + \mathrm{BD}_i + \mathrm{IF}$$

where

$$W_e = [\bar{\mathbf{v}}\cdot\boldsymbol{\tau}^w], \qquad W_i = [\hat{\mathbf{v}}\cdot\boldsymbol{\tau}^w]$$

$$B_e = -\langle \bar{\mathbf{v}}\cdot\nabla p\rangle, \qquad B_i = B - B_e$$

$$N_e = -\langle \rho_0\bar{\mathbf{v}}\cdot(\overline{\mathcal{L}\mathbf{v} + \mathbf{v}v_z})\rangle, \qquad N_i = -N_e$$

$$\mathrm{LF}_e = -\langle \rho_0 A_m\overline{\mathbf{v}\cdot\nabla^4\mathbf{v}}\rangle, \qquad \mathrm{LF}_i = \mathrm{LF} - \mathrm{LF}_e$$

$$\mathrm{BD}_e = -[\bar{\mathbf{v}}\cdot\boldsymbol{\tau}^b], \qquad \mathrm{BD}_i = \mathrm{BD} - \mathrm{BD}_e.$$

The nonlinear advective terms provide an exchange of kinetic energy between the internal and external components of the flow, but do not lead, in a mechanically closed basin, to a net increase in kinetic energy. In an ocean basin with variable topography (and density stratification), the work of pressure forces in the interior of the fluid lead to a conversion of potential energy (P) to kinetic energy of both components. In a flat bottom ocean, the pressure forces cannot do work on the external mode and $B_e \equiv 0$ (Holland 1975).

An indication of the adjustment process during the first two years of integration is given in Fig. 4. The basin-averaged kinetic energy per unit volume (K) (Fig. 4a) shows a rapid decrease during the first two months,

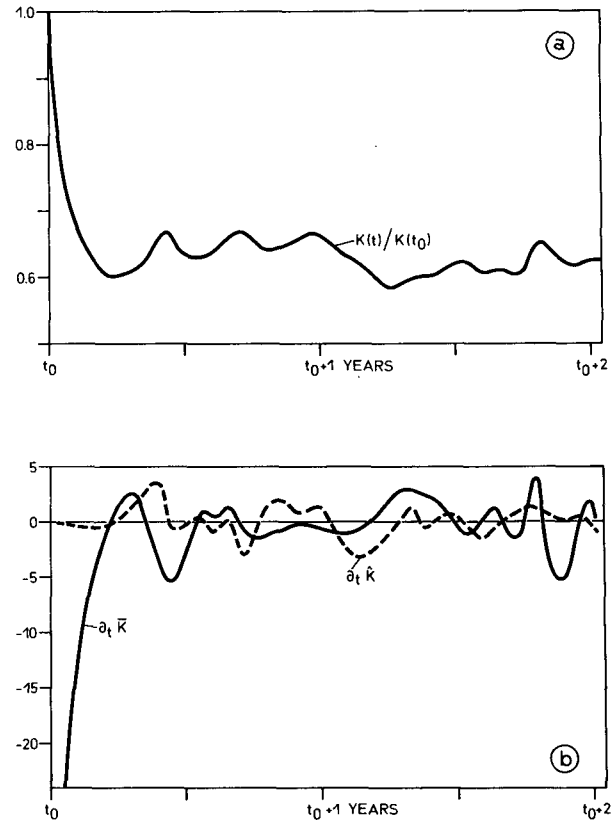

FIG. 4. Basin integrated kinetic energy vs integration time, normalized with the energy at the start of the experiment (a). The experiment is initialized at year 16 of the flat bottom case of C85. (b) Time-rate of change of energy associated with the external component (full line) and internal component (dashed line). Units: 10^{-7} erg cm^{-3} s^{-1}.

followed by an irregular oscillation around a mean value which is nearly 40% less than in the flat bottom case. Figure 4b shows the time-rate-of-change of kinetic energy separately for the vertically averaged, or external component of the flow field ($\bar{K}$), and for the internal component ($\hat{K}$). The rapid initial energy tendency appears as a consequence of the response of the external mode only; there is no net tendency of the internal component during the period of integration.

The work terms which determine the kinetic energy of the flow are shown as a function of time in Fig. 5. Throughout the period the work by the wind stress appears as the only forcing mechanism. The dominant sink is provided by the bottom drag, followed by the buoyancy work done by the pressure forces. Lateral friction of biharmonic form, included in the model for numerical reasons, i.e., to prevent a buildup of enstrophy at the smallest scales resolved by the grid, has only a minor influence on the overall energy balance. Also less important is the energy loss due to internal dissipation.

The work by the pressure forces provides the link between kinetic and potential energy (see also Fig. 6). The negative contribution to the kinetic energy budget reflects the effect of the wind-driven gyres on density stratification; it indicates a net negative correlation between vertical motion and temperature over the basin, i.e., upward motion is associated with denser water, sinking motion with less dense water. The transfer of kinetic energy has to maintain the potential energy of the system against the work of the buoyancy forces.

Due to their considerable fluctuations throughout the integration periods the work terms are in near balance only when averaged over at least 6–8 years. The strongest oscillations are exhibited by the buoyancy work and bottom drag terms with an indication of almost opposite tendencies. This behavior could indicate a vacillation between potential and kinetic energy of the system and may be interpreted as another manifestation of the low-frequency, gyre-scale oscillations revealed in C87.

The box diagrams (Fig. 6) show 8-year averages of the energy cycle between the reservoirs of potential energy (P), the kinetic energy of the external component ($\bar{K}$) and the kinetic energy of the internal component ($\hat{K}$), for the flat bottom case (Fig. 6a) and the rough bottom case (Fig. 6b). Wind energy is mainly received by the internal mode, whereas the most important energy sink is bottom drag, acting on the external mode. The link between $\hat{K}$ and $\bar{K}$ is provided by the pressure forces via the interaction with the reservoir of P. Here T represents the change of potential energy by the thermal forcing at the surface, and by diffusion and convection; values of T have been computed as residuals of the pressure work terms (which neglects the temporal variation of P). In the rough bottom case, 57.2% of the total kinetic energy received by the system as a whole is dissipated by bottom friction, 20.8% by buoyancy work, 14.4% by lateral friction, and 7.8% by interior friction. Overall, the box diagrams reveal only small differences between the energetic behavior of the two solutions. It seems that the energy flow along the

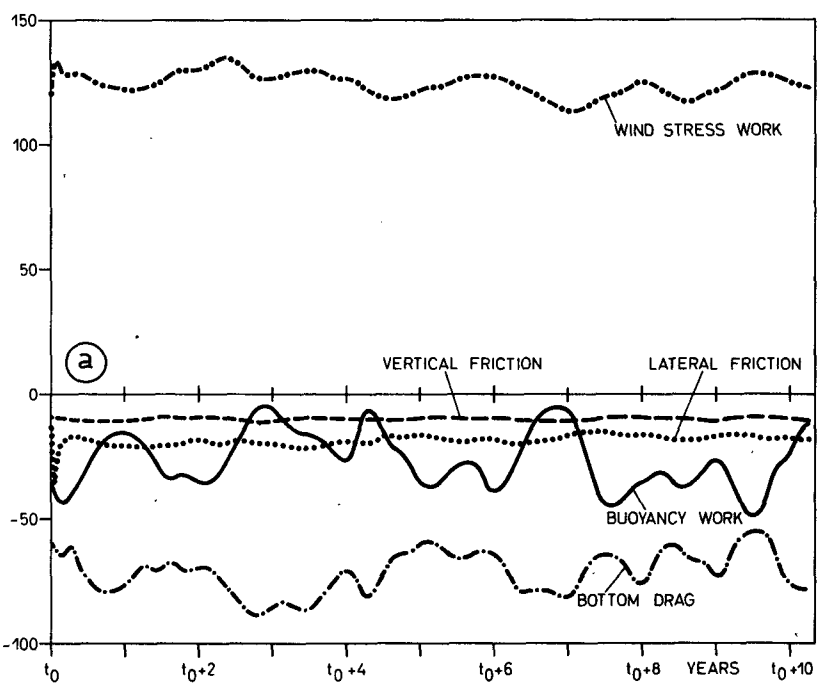

FIG. 5. Components of the kinetic energy balance of the model system as a function of time. Units: 10^{-7} erg cm^{-3} s^{-1}.

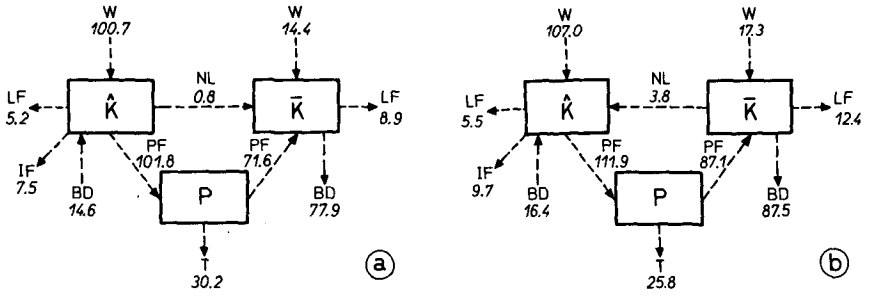

FIG. 6. Energy cycle, averaged over an 8 year period, between the kinetic energy of the vertically averaged flow ($\bar{K}$), the kinetic energy of the baroclinic component ($\hat{K}$) and the potential energy of the system (P), for the flat bottom case of C85 (a), and the rough bottom case (b). The directions of the energy transfers are indicated by the arrows. Units: 10^{-7} erg cm^{-3} s^{-1}.

main pathway $W_i - (\hat{K}) - (\bar{K}) - \mathrm{BD}_e$ has become somewhat stronger in the rough bottom case; the nonlinear transfer between $(\hat{K})$ and $(\bar{K})$ has changed its sign; lateral friction acting on the external mode increased about 40%.

Obviously, basin integrated budgets can only give limited information about the dynamics of the inhomogeneous flow in an ocean basin. Energy is concentrated near the western wall, and changes of the energetics in the interior can be masked by the energetics of the western boundary current. This can be seen especially in the pressure work on the external mode which can be nonzero only if topographic variations are present. In the "flat bottom" model this is the case only at the shelf along the western wall. Thus, PF_e must be concentrated there, and the relatively small difference between the solutions suggests that the main contribution to the budget is due to processes in the western boundary current where no bottom roughness has been introduced.

Some indications of the mechanism responsible for the strong decrease of the external energy taking place in the initial phase (Fig. 4) may be obtained by the energy transfer terms acting on the external mode during this time (Fig. 7). The strongest reaction after introducing the topography is shown by the lateral friction. The sharp increase of dissipation by the highly scale-selective biharmonic friction term may be understood as a consequence of the topographic scattering of the flow into smaller scales (e.g., see Fig. 14). Corresponding to the rapid decrease of $\bar{K}$, LF_e subsequently relaxes towards smaller values again, so that in the time averaged budgets its effect becomes obscured.

A comparison of the eddy energy patterns during different time intervals indicated that the main features of the fluctuating flow were well established after only a few years of integration with the rough bottom model. In the following discussion of the model results, the characteristics of the flow field in the period of years 5 to 11 of the rough bottom case will be compared with the period of years 18 to 24 of the flat bottom solution of C85.

4. Statistical mean properties of the flow

In this section, the characteristics of the six year mean values of the mean and fluctuating components of the flow field will be considered. As discussed by C85, the mean flow in the basin can be understood in terms of a thermohaline circulation driven by the differential heating at the surface, superimposed by a wind-driven double gyre pattern. The thermohaline aspect of the solution manifests itself by a northward (eastward) surface flow along the western and northern wall toward the main region of sinking motion in the northeastern part of the basin. The kinetic energy of the mean flow at the surface (Fig. 8) is dominated by the intense western parts of the wind-driven gyres. Maximum energies are associated with the western boundary current of the anticyclonic, subtropical gyre and the eastward, midlatitude current which separates it from the northern, cyclonic gyre. In the thermocline,

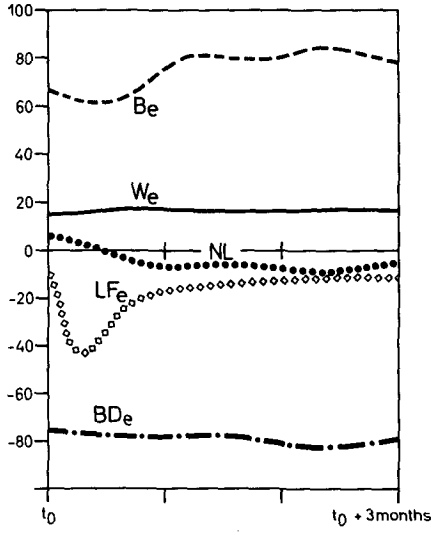

FIG. 7. Energy transfer terms acting on the external component of the flow during the first 3 months after introducing the rough topography. Units: 10^{-7} erg cm^{-3} s^{-1}.

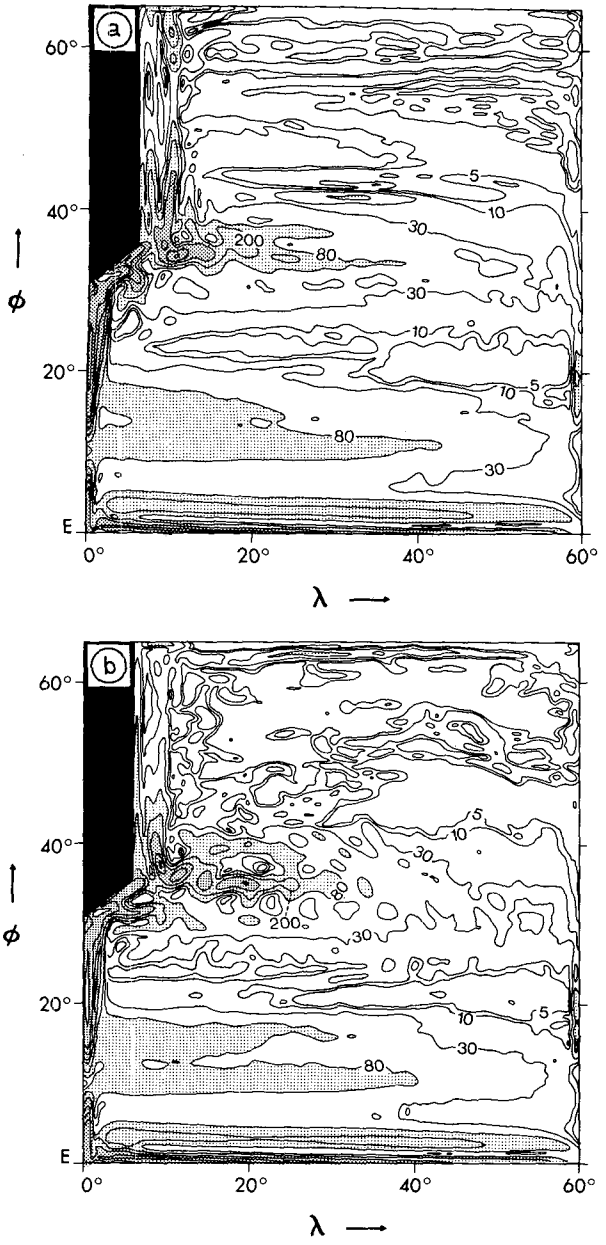

FIG. 8. Kinetic energy of the six-year mean flow at the surface (in $cm^2\ s^{-2}$), (a) flat bottom case; (b) rough bottom case.

the kinetic energy pattern of the rough bottom solution exhibits no fundamental departures from the flat bottom solution.

In both experiments the separated boundary current loses its character as a concentrated, energetic jet at a zonal distance of about 1500 km from the western wall. The penetration scale of the model jet, as well as that of the energetic segment of the associated eddy field are somewhat smaller than observed values for the Gulf Stream and Kuroshio Extension (Schmitz 1984; Schmitz et al. 1983). In an extensive sensitivity study, Holland and Schmitz (1985) demonstrated that the east–west scale of the midlatitude jet in a QG-model critically depends on a subtle balance of physical processes that affect the inertial character of the flow on the one hand and its energy loss due to instability mechanisms on the other. An interpretation of the present solution in terms of these results is not straightforward, however. The main difficulty in any model of the midlatitude ocean circulation is to achieve a proper separation of the western boundary current. In QG-models, the problem is typically circumvented by driving the model circulation by an antisymmetric wind stress pattern that readily produces a narrow, inertial jet at the $\text{curl}\tau = 0$ latitude. The approach is successful insofar as it produces an oceanlike interior circulation. However, the actual physics of the separation process may be quite different, involving both a strong baroclinicity of the jet and strong spatial changes in the underlying bathymetry.

The behavior of the flow field at the western wall indicates some basic problems of the present model with respect to the separation aspect. The western boundary current of the subtropical gyre does not leave the coast in a single, coherent band. Part of the current recirculates in a tiny subgyre; another part continues to follow the coast northward. The first feature may be an effect of the particular form of the western wall; the second may be explained in terms of the tendency of the thermohaline circulation to produce a northward flow along the subpolar extent of the western continental shelf. As a consequence, the volume transport (with a maximum of ~100 Sv (Sv $\equiv 10^6\ m^3\ s^{-1}$) near the separation site, reducing to ~50 Sv over a distance of about 1500 km to the east), the strength of the eastward current and its penetration scale all appear to be weaker than in quasi-geostrophic models forced by a similar wind stress amplitude.

Horizontal distributions of eddy kinetic energy (K_E) are shown in Fig. 9 for both the flat and the rough bottom case. The pattern of K_E at the near surface level (Fig. 9a, b) indicates the main instability regions of the thermocline flow. Maximum values (1000 to 1500 $cm^2\ s^{-2}$) are associated with the western boundary current and the midlatitude eastward current. In addition, a band of moderate eddy activity extends along the westward flowing portion of the subtropical gyre. There are only small differences between the solutions in the thermocline pattern of K_E in these energetic regions. Thus, in addition to the upper layer mean flow, also the instability properties of the model seem not to be affected by the introduction of the small-scale bottom roughness. The differences in the vertical structure and the space–time characteristics of the fluctuations discussed below can thus be assumed to reflect direct effects of the topography on the eddy dynamics.

An indication of a topographic influence appears in the significant reduction of K_E in the midlatitude

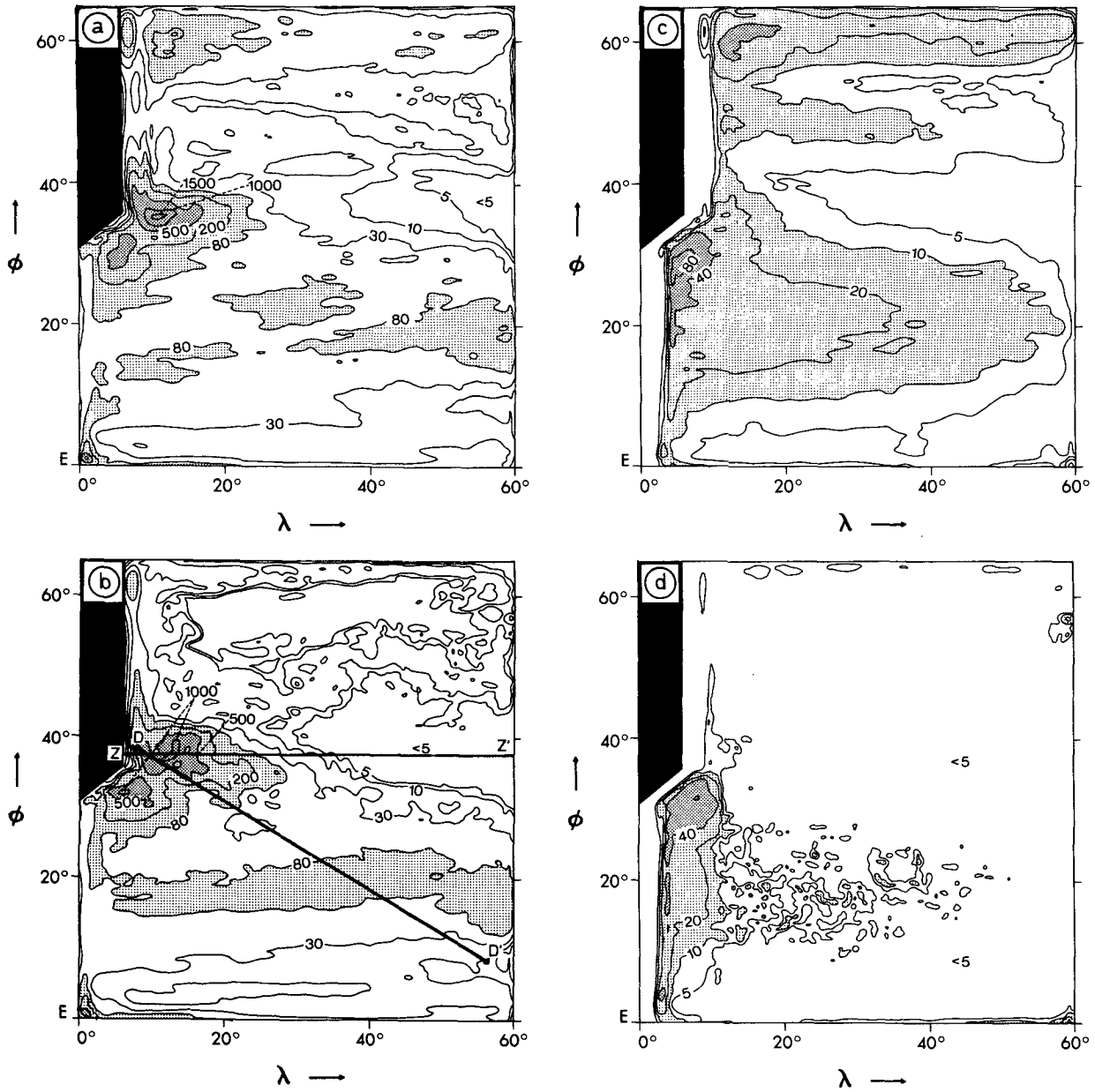

FIG. 9. Mean kinetic energy of the eddy field at the surface of the flat (a) and rough bottom case (b), and in 1414 m of the flat (c) and rough bottom case (d). Units: $cm^2\ s^{-2}$.

energy minimum, which characterizes the solutions in the eastern half of the basin, i.e., along the extension of the eastward current. The gradients of K_E toward the energetic instability areas are much stronger in the rough bottom case, indicating that energy is less effectively radiated away from the source regions.

A strong influence of the bottom roughness appears in the pattern of deep K_E (Fig. 9c, d). In the flat bottom case, a considerable amount of eddy energy finds its way from the subtropical thermocline into deeper levels. In the gyre interior, the tendency toward barotropy is substantially reduced in the rough bottom case. More intense deep energies are now entirely confined to the westernmost part of the subtropical gyre (where the topographic structure was not altered).

To illustrate the influence of topography on the depth dependence of eddy intensity, vertical sections of K_E are presented in Fig. 10. (The sections are indicated in Fig. 9b.) The zonal section ($Z - Z'$) approximately follows the axis of the midlatitude eastward current and covers the transition from the energy maximum associated with the concentrated jet to the region

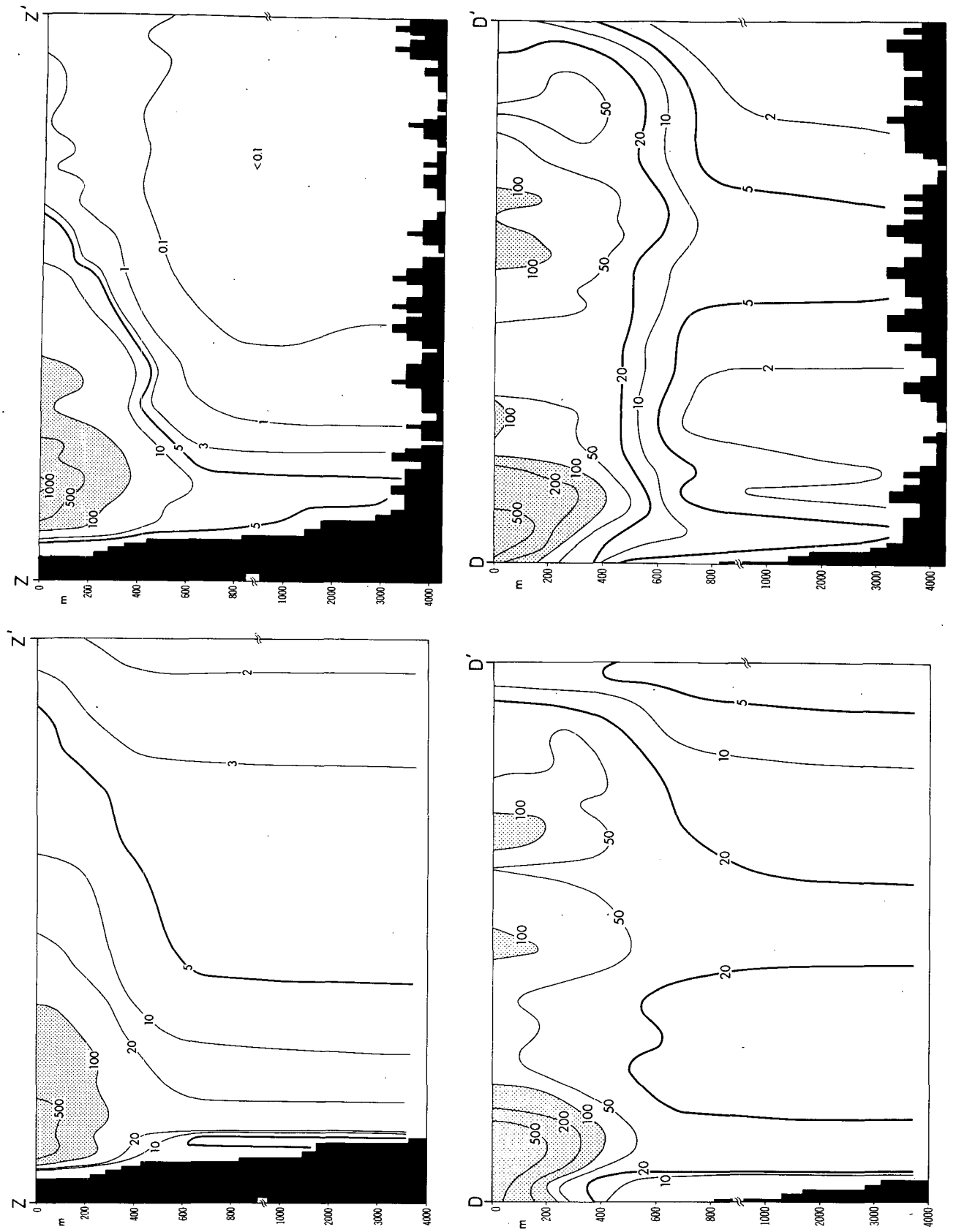

FIG. 10. Sections of eddy kinetic energy along the lines $Z - Z'$ and $D - D'$ indicated in Fig. 9b for the flat and rough bottom case.

of very weak energy in the east. The northwest–southeast section ($D - D'$) encompasses both instability regions of the subtropical gyre as well as the zone of lower energy in between. Both model cases exhibit qualitatively the same K_E pattern. Below the thermocline maxima (about 1000 $cm^2 s^{-2}$ in the eastward jet and about 100 $cm^2 s^{-2}$ in the gyre interior) eddy energy reaches down to the bottom, creating characteristic bowl-shaped structures. It is not the shape of this pattern, but the intensity of the deep-eddy field which differs in the two model realizations. Below the thermocline maxima, eddy energy is reduced by a factor of about 4 in the rough bottom case; in the less energetic regions the decrease seems to be much stronger.

The effect of bottom roughness is expected to be stronger in regions of weaker flow intensity. According to the theoretical scenario outlined earlier, the tendency to barotropy produced by nonlinear intermodal energy exchanges should be more strongly inhibited the smaller the ratio Ro/δ. Rhines et al. (reported in Dickson 1983) tried to rationalize the observed, geographically greatly varying depth dependencies of oceanic eddy fields in terms of this framework. Instead of Ro, the velocity scale $U_E = (2K_E)^{1/2}$ of the thermocline flow variability was used as a measure of the local eddy intensity. The ratio of K_E in the thermocline to K_E in a deep layer was taken as a proxy of the vertical structure. When the depth dependencies of all long-term North Atlantic current meter observations were plotted against U_E/δ (δ = rms-depth variation in a certain area around the moorings), a picture emerged which appeared grossly consistent with the theoretical prediction (Fig. 11). As the considerable scatter makes clear, the local effects of nonlinearity and topography cannot be expected to explain more than some part of the actual depth dependence. There is evidence, however, that the depth dependence is weaker in intense flows over smooth topography and vice versa.

A similar approach can be taken to illustrate the effect of the model topography (Fig. 12). A scatter plot of the ratio K_E (in 300 m) to K_E (in 3000 m) as a function of the flow intensity U_E for "stations" regularly distributed over the subtropical gyre of the flat bottom case is given in Fig. 12a. The pattern is in sharp contrast to the observed behavior: the depth dependence of eddy energy increases with increasing flow intensity. This behavior may be explained by noting that in a flat bottom case the barotropization tendency due to the nonlinear energy exchanges is opposed only by the instability mechanism, which provides a source of K_E in the thermocline. The instability regions can be identified as the stations with higher U_E. As shown by C87, eddy energy is radiated away from these regions primarily in the barotropic mode. Thus, in the less energetic, stable areas, i.e. at stations with smaller U_E, the depth dependence is weak.

The introduction of topography changes this behavior completely. In Fig. 12b the depth dependencies have

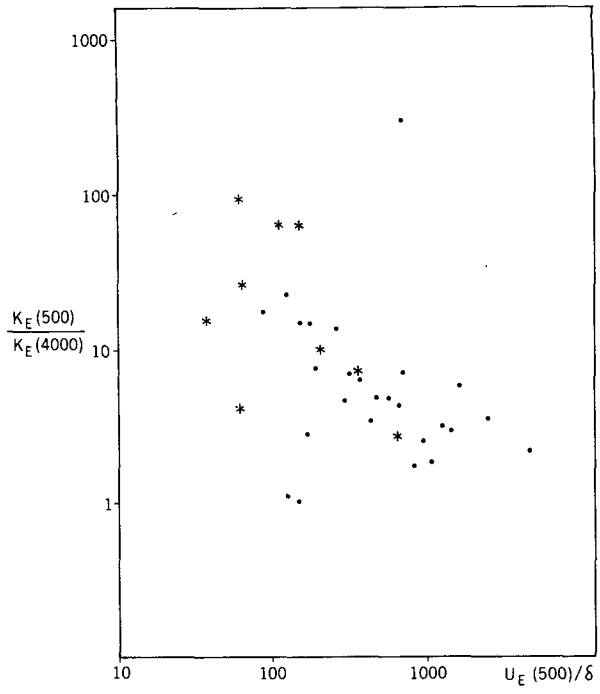

FIG. 11. Ratio of eddy kinetic energy (K_E) in the thermocline (~500 m) of the North Atlantic to energy in the deep ocean (~4000 m), plotted against U_E/δ where $U_E = \sqrt{2K_E}$ represents a measure of flow intensity in the thermocline and δ is the topographic roughness parameter. Dots indicate current meter observations in the western, asterisks in the eastern NA (according to Dickson 1983).

been evaluated at the same points within the subtropical gyre as in the flat bottom case. For simplicity, we regard the roughness parameter as constant over the basin, i.e., $\delta = 0.1$. Therefore the energy ratio may be plotted against U_E as well as against U_E/δ, which enables a comparison both with the flat bottom case as with the observational result. The main feature to be noted is that the tail of more and more barotropic flow away from the instability areas completely disappears. It seems that the vertical structure is less affected in regions of higher U_E so that there is some tendency toward a more depth-dependent structure in less intense flow regions as has been found in the observations. However, the strong scatter indicates that there is no functional relationship between the vertical eddy structure, the local intensity of the flow, and the topographic roughness.

5. Space-time structure of the instantaneous flow

A snapshot of the flow field in the subtropical gyre is given in Fig. 13 for the flat bottom, and in Fig. 14 for the rough bottom experiment. In both cases the actual flow pattern in the thermocline is dominated by eddy structures of 200–300 km scale, with maximum velocities of 20–30 cm s^{-1}. There is a striking difference, however, in the vertical structure of the eddy field: the

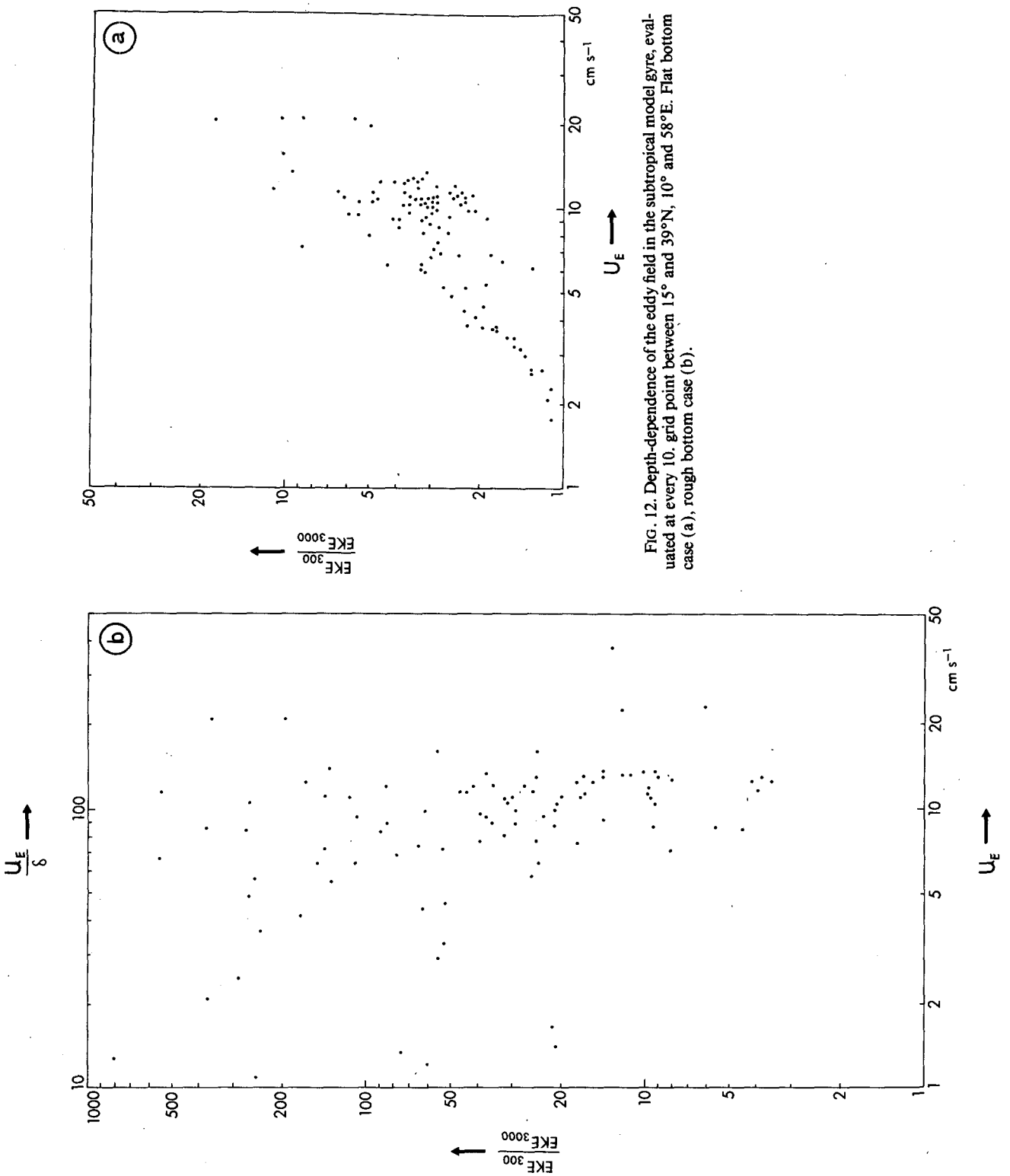

FIG. 12. Depth-dependence of the eddy field in the subtropical model gyre, evaluated at every 10. grid point between 15° and 39°N, 10° and 58°E. Flat bottom case (a), rough bottom case (b).

vertical coherence is high in the flat bottom case (the horizontal scales are similar in all levels, but the velocities decrease by a factor of 2–3). Accordingly, there is an intense vertically integrated transport (40–50 Sv) associated with single eddies, as revealed by the streamfunction contours of the external mode (Fig. 13a). In the rough bottom case, the flow below the thermocline shows no resemblance to the upper layer eddies. The whole water column below about 1000 m appears to be topographically controlled and reflects the kinematical constraints imposed by the bottom bumps (Figs. 14c, d). The depth-integrated volume transport associated with the synoptic-scale eddies is greatly reduced and does not exceed 10–20 Sv (Fig. 14a).

The space–time characteristics of the flow field are illuminated in Figs. 15 and 16. The phase diagrams show the deviation of the meridional velocity component from its 6-year mean value as a function of longitude and time along a section at 20° latitude, i.e. in the band of moderate eddy activity.

In the flat bottom case we find a rather regular pattern of westward propagating waves in the deep level (1414 m). The predominant east–west wavelength is about 520 km, the phase speed of the waves is 13 to 14 cm s^{-1}. In the thermocline level (224 m), a similar wave pattern is visible again, but intermittently superimposed by more energetic, isolated structures. The propagation characteristics of the background wave field and of the energetic features seem to be quite different. The wave signal shows phase speeds of about 12 cm s^{-1} (on a background mean westward flow of 2–3 cm s^{-1}), similar to the behavior in the deeper levels. Predominant wave lengths are about 450 to 500 km, somewhat smaller than in the deep ocean. The propagation characteristics compare favorably with the phase speed of Rossby waves in the first baroclinic mode, though the vertical structure indicates the significance of energy transfer into the barotropic mode. (A more detailed discussion of the propagation characteristics is given by C85.) The fluid velocities associated with the wave pattern are generally less than 10

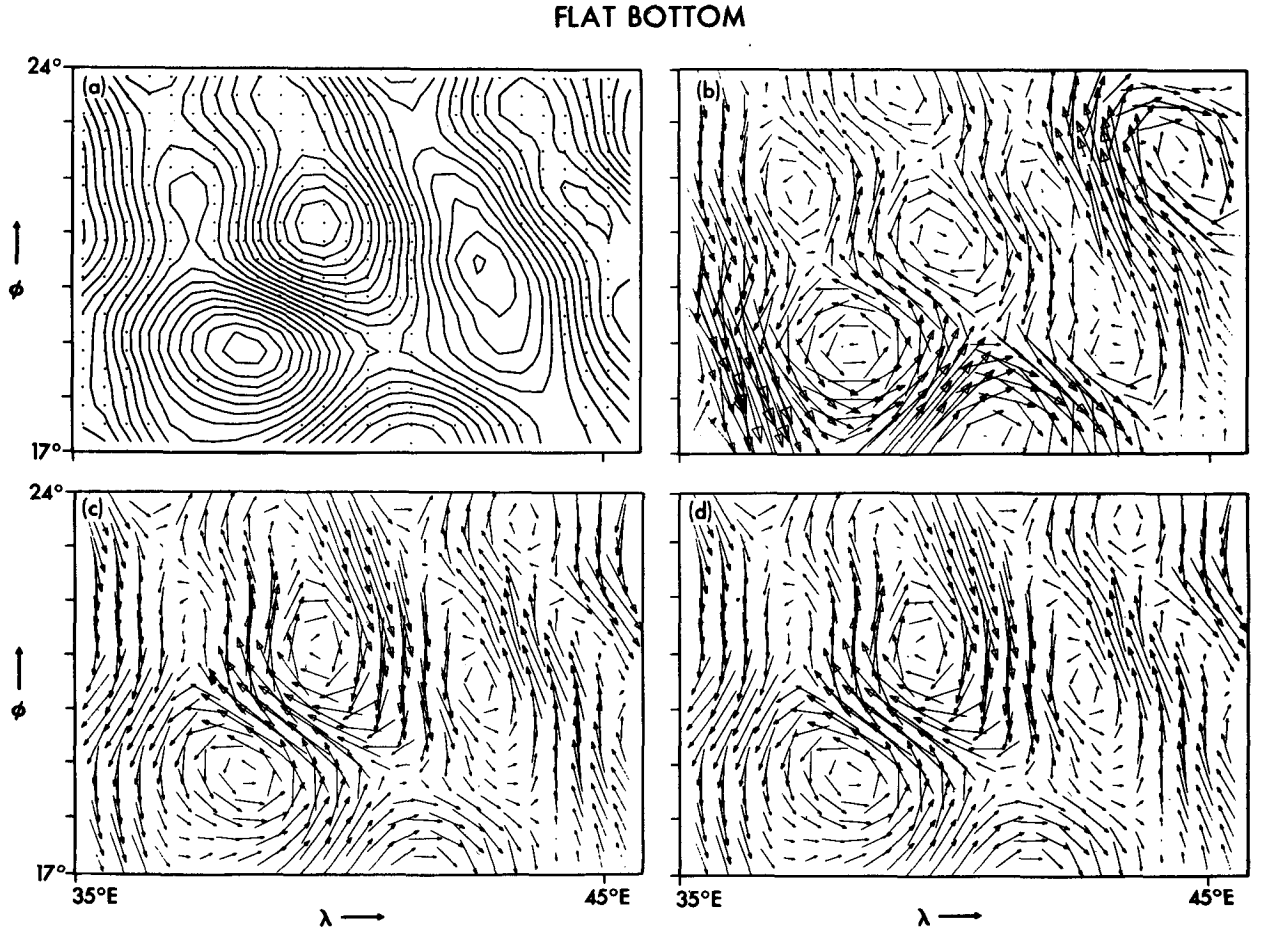

FIG. 13. Instantaneous velocity field in the flat bottom case: streamlines of the external mode, CI = 5 Sv (a), horizontal velocity in the thermocline (224 m) (b), in 1414 m (c), in 2877 m (d); A vector of 1° length corresponds to 20 cm s^{-1} (b), 10 cm s^{-1} (c), 10 cm s^{-1} (d).

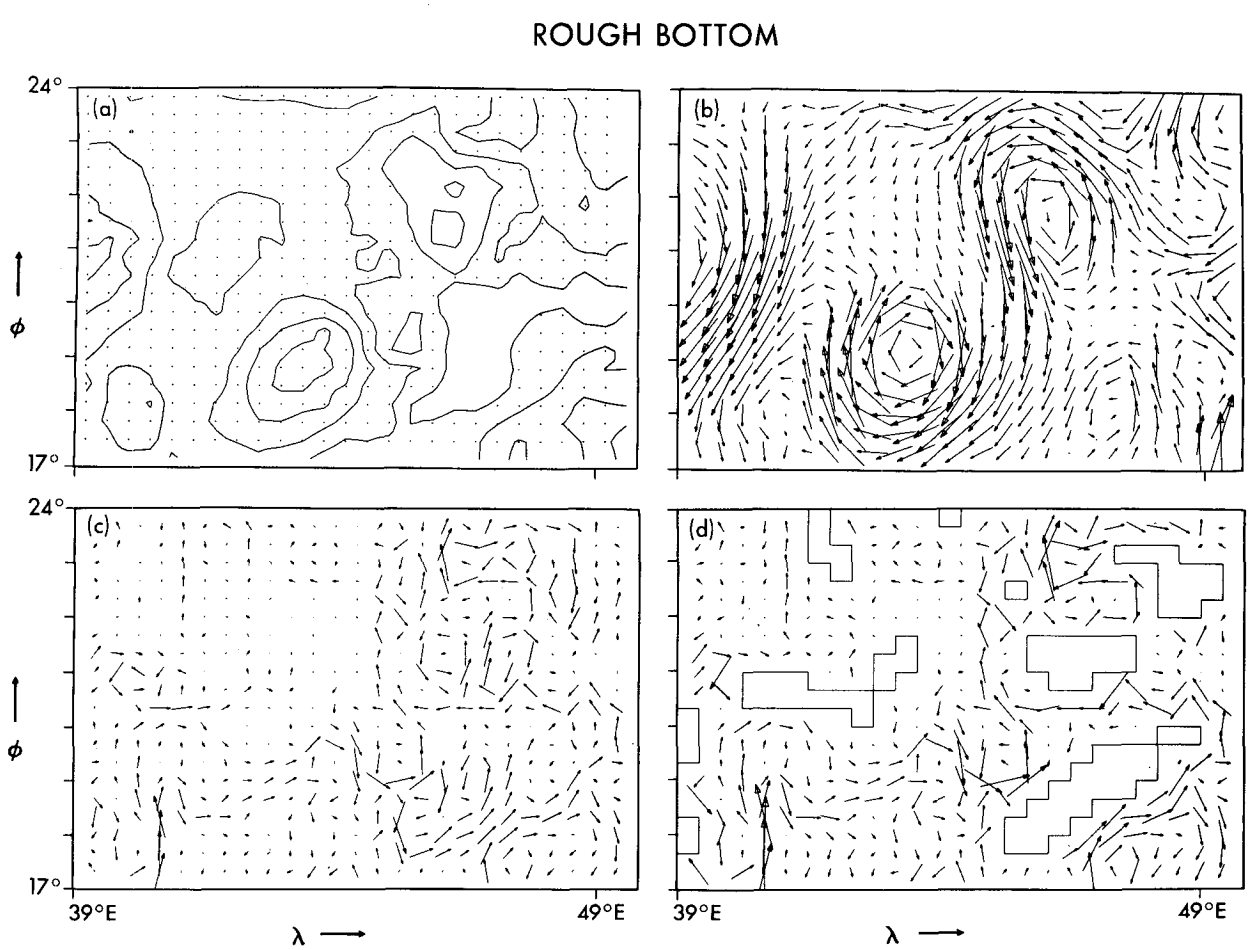

FIG. 14. Instantaneous velocity field in the rough bottom case; depths and scales as in Fig. 13, except for (d) with a vector scale of 7 cm s^{-1}.

cm s^{-1}. The wave steepnesses less than unity suggest an interpretation as a field of weakly nonlinear Rossby waves.

Occasionally, energy in the thermocline becomes much more concentrated: singular energetic structures show fluid velocities of 20–30 cm s^{-1}. There is a general tendency of significantly lower phase propagation of these features relative to the wave signal; typical phase speeds are about 6 cm s^{-1}. Since particle velocities exceed the phase velocity several times, nonlinear effects can be expected to play a much more important role here. Energetic vortices in the flat bottom case are not of long duration, however. A closer look at the sequence of these events hints at the interaction with the deep flow as an essential element of the process that terminates the identity of a thermocline eddy. Near the end of an eddy life cycle, the flow always seems to intensify strongly in the lower layer, indicating a downward transfer of energy. The flow fields in the upper and lower layers lock together, followed by rapid removal of energy by wave dispersion.

Figure 16 shows the phase diagram for the topography case. There are striking differences both in the deep and in the thermocline level relative to the flat bottom case. Below the thermocline, wave propagation has completely ceased (except for the westernmost part which corresponds to the area where no topographic variability was introduced). The flow scales are smaller and show characteristics of standing waves, apparently locked to the topographic contours.

In the thermocline, westward phase propagation is still prevalent, but instead of an interactive wave field the velocity fluctuations have much more the character of phase-coherent noninteracting vortices with rather weak flow in between. This change in behavior relative to the flat bottom case is also apparent when the propagation speeds are compared; the energetic structures in this example move with speeds of 6–7 cm s^{-1}, much slower than the Rossby waves in the flat bottom experiment. In fact, there seems a close similarity in the propagation characteristics of these vortices to the intermittent energetic events seen before. No significant difference is apparent between the fluid velocity of these structures in both experiments; the novel feature is that

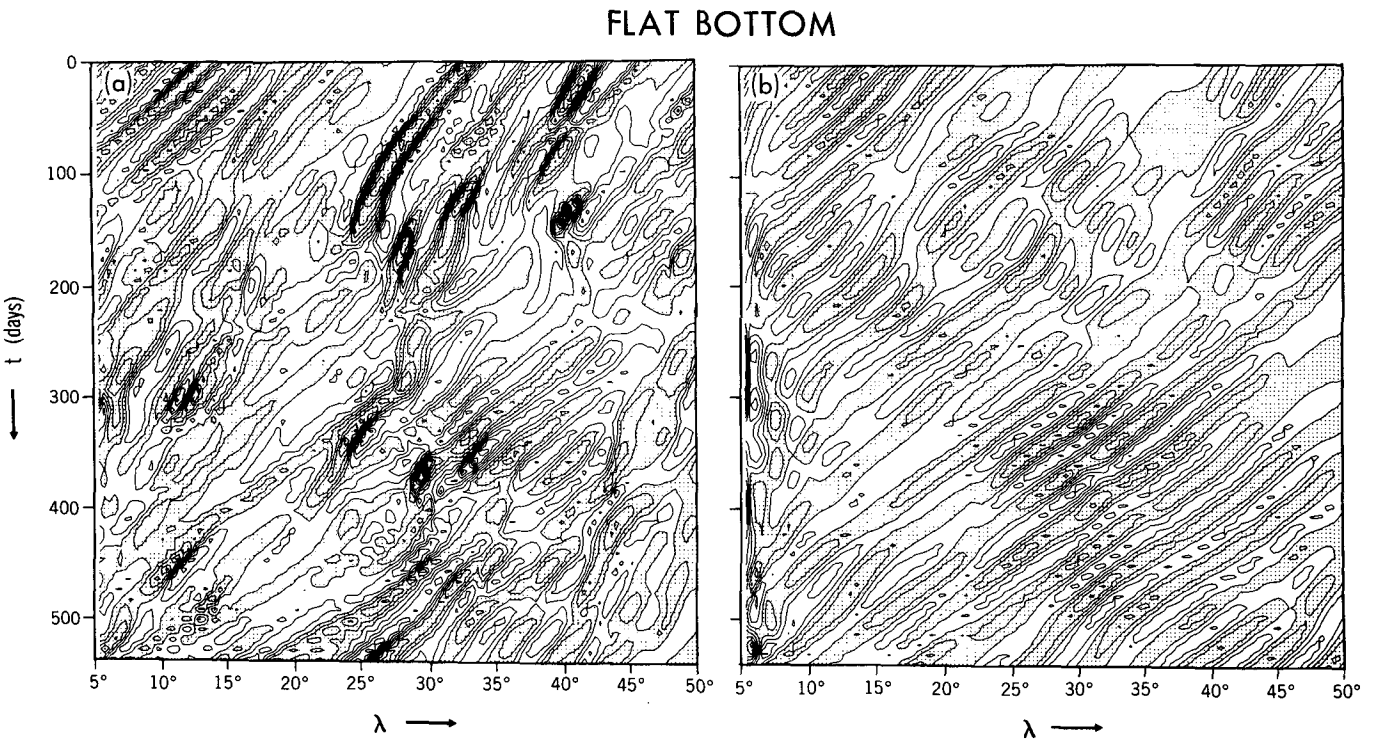

FIG. 15. Longitude–time plot of the meridional perturbation velocity component v' at $\Phi = 20°N$, for a thermocline level (224 m) (a) and a deep level (1414 m) (b); contour intervals 5 cm s^{-1} (a), and 4 cm s^{-1} (b); stippling denotes southward flow.

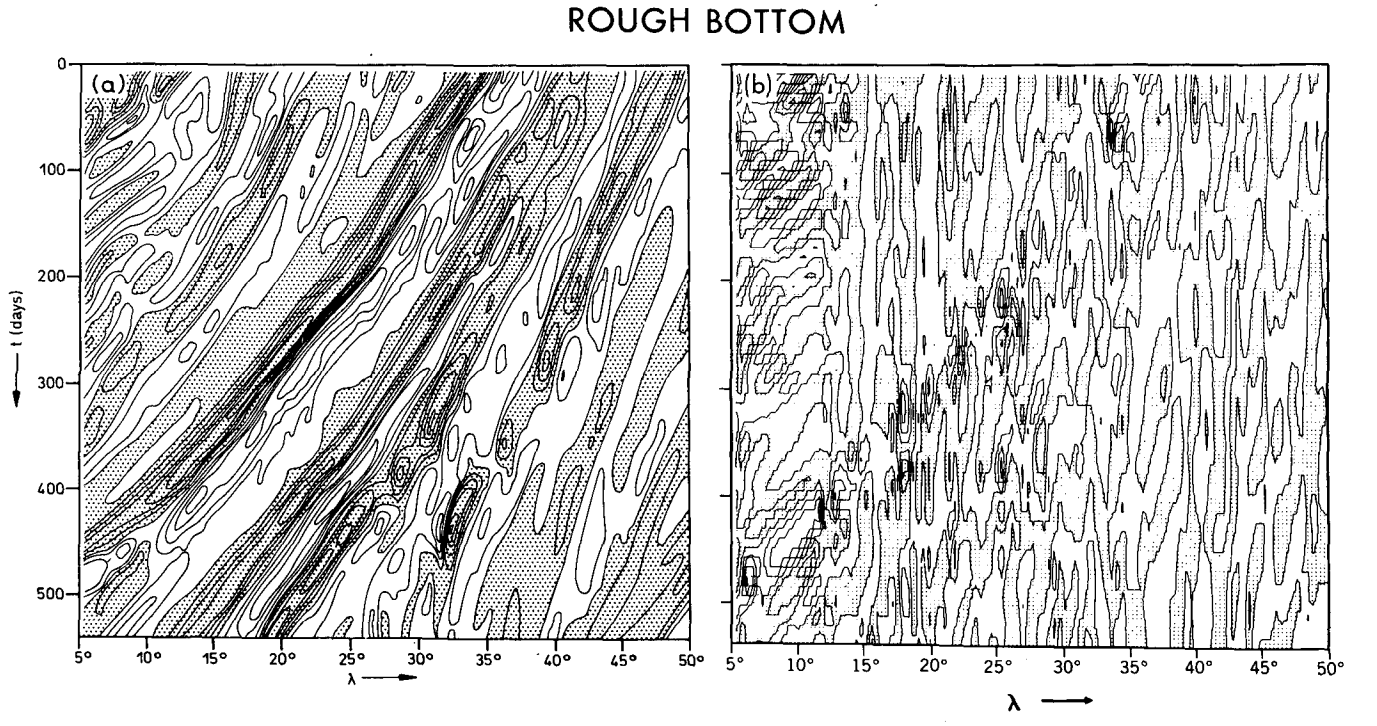

FIG. 16. As in Fig. 15, but for rough bottom case.

in the rough bottom case they retain their identity over a much longer period of time.

Following the discussion of the flat bottom behavior, we might explain this stabilization as a consequence of the cessation of the coupling between upper and lower layer flow, which appeared to precede the radiation of energy by wave processes. The tendency of the downward energy transfer to create vertically coherent structures is effectively interrupted by the topographic scattering taking place. A signature of the strong thermocline eddy is visible in the deep level by intermittent patches of higher energy, indicative of the competition between the nonlinear tendency toward barotropy and the topographic scattering.

The energetic feature in the example of Fig. 16 represents a thermocline eddy which can be followed for about 1.5 years with only small modulations in amplitude, demonstrating the almost perfect containment of wave dispersion. Eddy lifetimes of 1 or 1.5 years were found to be typical by scanning through a six-year time series of flow data which also indicated a preference of anticyclonic vortices among these long-living structures in the subtropical gyre. Though a similar number of cyclonic eddies are generated by the instability process, they seem to lose their identity much more rapidly due to eddy–eddy interactions.

6. Low-frequency behavior and particle dispersion

The actual flow field in both experiments is dominated by a series of mesoscale eddies of rather isotropic character (Figs. 13 and 14); there is no significant difference between the zonal and meridional velocity variances. As has been demonstrated in C87 for the flat bottom case, this is not true for the low-frequency part of the velocity spectrum. The low-pass filtered component of the time variant flow showed a marked tendency to elongated zonal bands in the external mode, a manifestation of the energy decascade in homogeneous, quasi-geostrophic turbulence.

In order to evaluate the effect of bottom roughness on this process, a similar analysis as in C87 was performed in the present experiment. The time series of the streamfunction variations, $\psi' = \psi - \bar{\psi}$, where $\bar{\psi}$ denotes the time–mean component, has been low-pass filtered using the same digital filter as in C87, i.e., all periods shorter than about 4 months were eliminated. A snapshot of the filtered time series ψ_f' is given in Fig. 17. Compared with the corresponding result of the flat bottom model (Fig. 12(b) in C87) the pattern is completely different: the bandlike structure in the external mode has disappeared. The same is not the case for the low-frequency flow field in the thermocline. Figure 18 displays a meridional section of the filtered, zonal velocity component. Whereas the pattern is rather irregular and small-scale below ~700 m, a sequence of alternating easterly and westerly currents of O(2 cm s^{-1}) appears with a meridional scale of about 200 km.

Information on the character of slowly oscillating oceanic transients may be extracted from observations of freely drifting buoys. The dispersion behavior of fluid particles is heavily weighted by the low-frequency part of the velocity spectrum, as suggested by the spectral form of Taylor's theorem (which holds for the case of homogeneous turbulence). If the Lagrangian velocity spectrum is denoted by $\Phi(\omega)$, the displacement covariance of fluid particles is given by

$$D_{ij}(t) = \int_0^\infty (\Phi_{ij}(\omega) + \Phi_{ji}(\omega))g(\omega, t)d\omega$$

(Kampé de Fériet 1939). The contribution of the spectral components to the dispersion is weighted by

$$g(\omega, t) = \frac{\sin^2\omega t}{\omega^2/2}.$$

Since

$$\lim_{\omega t \to \infty} g(\omega, t) = \pi t\delta(\omega)$$

the dispersion process for larger spreading times t is dominated by low-frequency oscillations with $\omega < O(1/t)$ (Colin de Verdière 1983).

Indications of a slightly anisotropic dispersion behavior ($D_{xx} > D_{yy}$) have repeatedly been found in observations of drifting buoys (Rossby et al. 1983; Riser and Rossby 1983; Krauss and Böning 1987). It seems, however, that this behavior is confined to the oceanic thermocline; the spreading of deep floats is rather isotropic (e.g., Freeland et al. 1975; Böning 1988).

A Lagrangian analysis of the numerical model in the flat bottom version was recently performed by Böning and Cox (1988). The particle spreading in the interior of the subtropical gyre showed a moderate anisotropy in the thermocline, but a very strong anisotropy in deeper levels, i.e., the dispersion below the thermocline appeared as purely zonal and the meridional diffusivity ($K = D/2$) was not significantly different from zero. In this way the zonal barotropic bands manifest themselves in the Lagrangian framework.

The Lagrangian experiment has been repeated in the present, rough bottom version of the model. Details of the particle seeding and integration procedure are given in Böning and Cox (1988) and will not be repeated here. In order to compare typical Lagrangian characteristics of the model transients, we shall concentrate on the particle behavior in the interior of the subtropical gyre, i.e., in the band of moderate eddy activity in the westward flowing portion of the gyre.

Figure 19 indicates the vertical dependence of the rms velocity components and the single particle diffusivities for both the flat and the rough bottom case. (Each dot represents an average over ten realizations with 144 particles each.) There are no significant differences between the experiments in the upper, thermocline levels. Below the thermocline, the eddy ve-

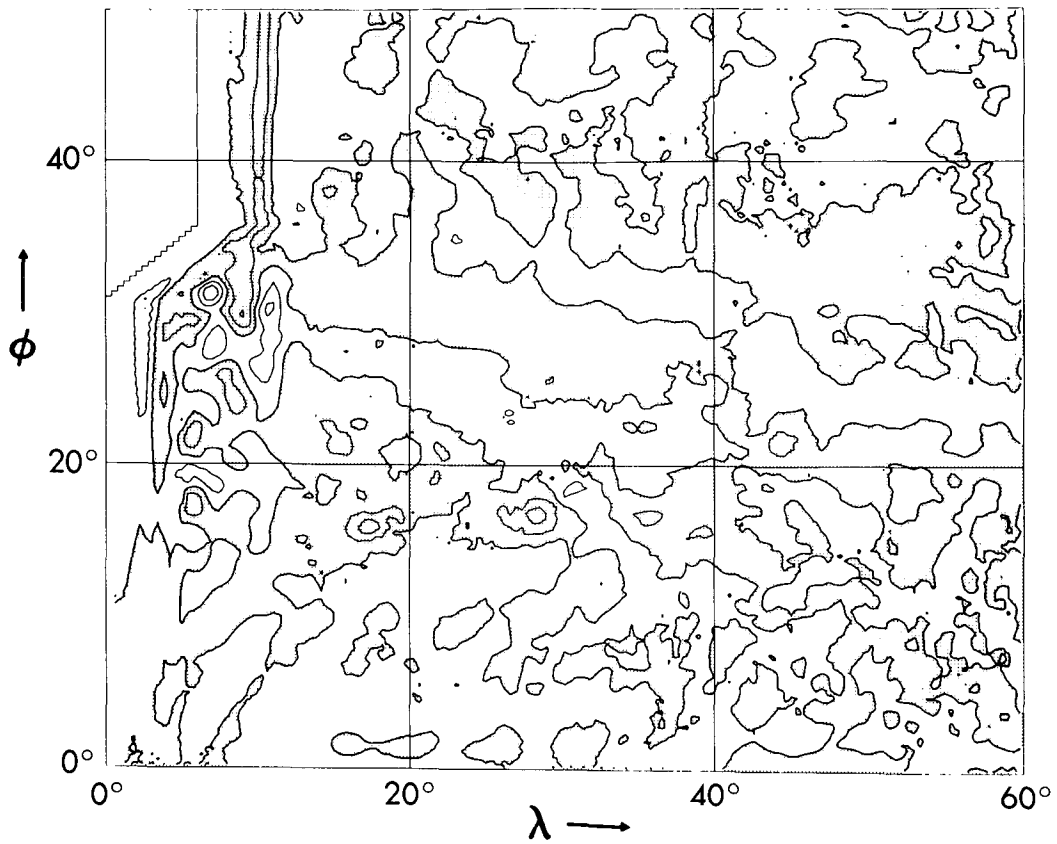

FIG. 17. Low-pass filtered, instantaneous mass transport streamfunction for the rough bottom case. Contour interval is 20 Sv.

locities decrease relative to the flat bottom case, as was found earlier in the Eulerian analysis. A major change occurs in the dispersion behavior; the strong anisotropy of the flat bottom model is replaced by a rather isotropic spreading in the rough bottom case. The fact that K_y increases while K_x decreases indicates a complete change of the character of the deep flow: the wavelike nature of the fluctuations in the flat bottom case, with particles oscillating meridionally without much net dispersion, changes to a more turbulent behavior with $K_x \approx K_y$.

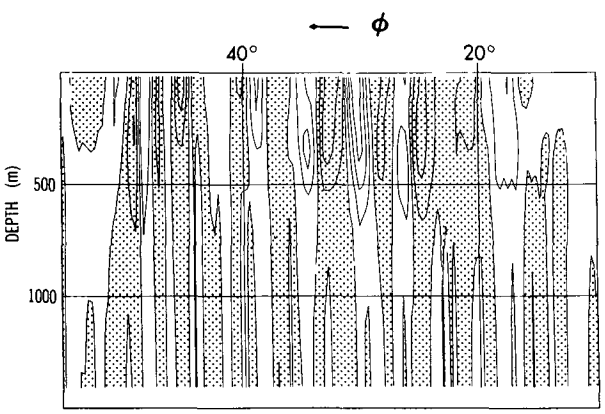

FIG. 18. Low-pass filtered, zonal velocity component evaluated at $\lambda = 20E$. Contour interval is 1 cm s^{-1}, stippling denotes westward flow.

A comparison of the model behavior with float observations was attempted by Böning and Cox (1988) on the basis of the normalized diffusivities, K_x/u' and K_y/v'. The strongest discrepancies were found in the deep levels where the oceanic "mixing lengths" are O(20–30 km) and rather isotropic whereas the model spreading was strongly anisotropic (Fig. 20). The deep length scales in the rough bottom case are closer to the oceanic values. (The quantitative correspondence between model and observations may be fortuitous and should not be overemphasized; from this single experiment we do not know, e.g., how these scales depend on the—prescribed!—topographic scales.) An anisotropic dispersion behavior [with $L_x \approx (2\text{–}3)L_y$] is confined to the thermocline in the rough bottom case.

7. Discussion

Bottom topography may be thought of as influencing the field of oceanic flow variability in two ways. The

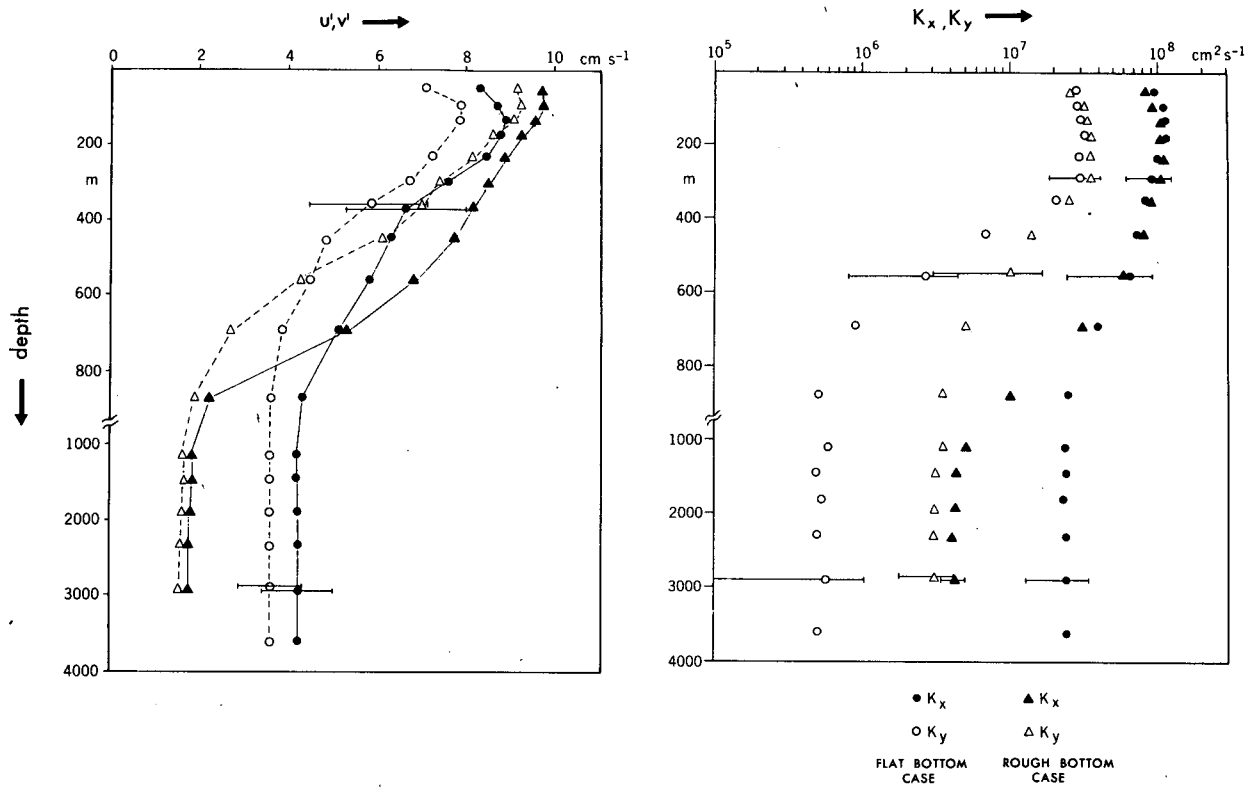

FIG. 19. Lagrangian statistics of the eddy field in the interior, westward flowing portion of the subtropical gyre: (zonal, meridional) components of rms velocities and single particle diffusivities in the flat bottom (●, ○) and rough bottom case (▲, △).

large-scale form of the ocean floor constitutes basic steering contours for the basin-scale, "mean" circulation whose instability provides the most important source of eddy variability. The focus of the present study was on the direct influence interactions of the deep current fluctuations with synoptic-scale irregularities of the ocean floor exert on the structure of the eddy field. Effects of bottom roughness have previously been investigated with QG models of decaying or wind-forced geostrophic turbulence in spatially homogeneous, open ocean areas, most recently in the extensive study of Treguier and Hua (1987, hereafter TH). The experiment reported here adds mainly two aspects: 1) it is concerned with the strongly inhomogeneous eddy field generated by the instability of the circulation in an ocean basin, and 2) it is based on a primitive equation, instead of a QG model.

The main effects of bottom roughness found by TH were an energy transfer from larger to smaller scales and a surface intensification of the eddy field. Treguier and Hua show that the enhancement of baroclinicity in the rough bottom solution is caused by an adjustment of the dynamics rather than by a direct barotropic–baroclinic energy transfer. An enhancement of the baroclinicity of the eddy field also constitutes an essential element of the present solution. In contrast to the turbulence experiment of TH, the main factor in the present circulation model is a strong decrease of the deep eddy kinetic energy whereas the energy level in the thermocline remains almost unaffected. The energetic adjustment after initialization of the topography experiment is dominated by a strong response of the external mode; eddy energy in the thermocline is essentially unchanged in the new equilibrium state. Eddy energy finding its way into the deep layers is rapidly "scrambled" into smaller, topographic scales and more effectively removed by the scale-selective friction.

An important aspect of the altered vertical structure is the decoupling of the fluctuating field into two, rather independent flow layers with completely different horizontal scales and propagation characteristics. The topographic constraint on the bottom flow is communicated through the whole water column below the thermocline. No remnants of the synoptic-scale eddies appear in this layer: the downward transfer of the eddy energy seems too weak to compete with the strong topographic control of the flow.

A rather unexpected feature of the model is the pronounced tendency of the thermocline fluctuations to form intense ringlike vortices, even in the eastern part of the subtropical gyre, away from strong boundary currents. Whereas in the flat bottom case strong vortices are quickly destroyed by wave radiation, they are able to keep their identity for a much longer duration in

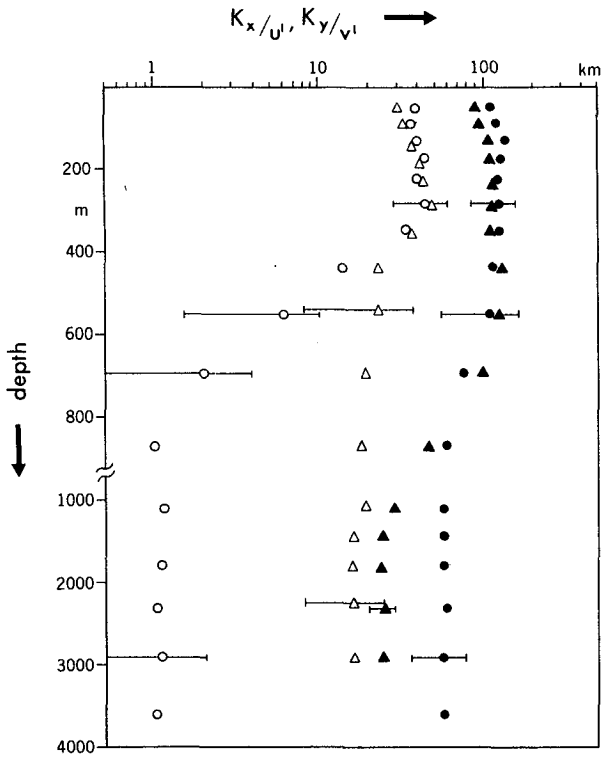

FIG. 20. Single particle diffusivities (zonal, meridional) normalized by the rms velocities for the flat (●, ○) and rough bottom (▲, △) experiment in the interior subtropical gyre.

the rough bottom solution. Since there is no direct topographic influence on the thermocline flow, a tentative explanation is based on the idea that the decoupling of the flow layers reduces the radiation of energy by wave processes. In the flat bottom case, the barotropization of the eddies is quickly followed by strong wave dispersion. By inhibiting this mechanism, bottom roughness may have an important indirect effect on the structure of the thermocline eddies.

The occurrence and stability of isolated, coherent vortices in actively cascading geostrophic turbulence has been demonstrated by McWilliams (1984). Under quasi-geostrophic dynamics, isolated vortices can emerge from random initial conditions, if $\beta = 0$ (or small). The QG vortices exhibit no parity bias and are passively advected by the larger scale flow.

There are some aspects of the strong eddies in the present, primitive equation calculation which suggest that QG theory might not be applicable. Their rather large scales together with particle speeds of 20–30 cm s^{-1} indicate the importance of vertical density advection. If the nonlinear divergence due to interface displacements becomes effective, elements of the intermediate-geostrophic (IG) regime (Charney and Flierl 1981; Yamagata 1982) could constitute an important part of the dynamics. Intermediate motions occur near the scale $L_I = (L_D^2 L_B)^{1/3}$ where L_D represents the Rossby radius and $L_B = f/\beta$. The dynamics of IG motions are characterized by a balance of nonlinear divergence due to interface displacements and wave dispersion. Thus, long-lived, phase-coherent vortices appear as the fundamental form of motion at these scales. These vortices are based on solitary Rossby waves with westward propagation close to $c = \beta L_D^2$ (Williams 1985). The existence of the IG solutions and their high stability in a broad range of mean flows has been demonstrated by Williams and Yamagata (1984) in a shallow water model. In a subsequent study, Williams and Wilson (1988) investigated the emergence of IG vortices and their coexistence with QG turbulence.

Several characteristics of the strong eddies in the present, primitive equation model appear close to the predictions of IG dynamics. Taking $L_D = 50$ km as a representative value of the first baroclinic Rossby radius in the subtropical thermocline (C87), $f = 5 \times 10^{-5}$ s^{-1}, $\beta = 2.2 \times 10^{-13}$ cm^{-1} s^{-1}, the theoretical IG scale is about $L_I \sim 200$ km (at $\phi \sim 20°$), and the IG propagation speed $c \sim 5.5$ cm s^{-1}. Though it is not obvious how to interpret the size of an isolated vortex in terms of the length scale, the intense eddies found in the model characterized by a diameter of about 300 km and westward propagation with 6–7 cm s^{-1} (on a mean flow of about 2–3 cm s^{-1}) are not inconsistent with the assumption that they might represent a PE model analogue to the hypothesized IG vortices.

The focus of this study has been on the effects of a variable topography on the fluctuating part of the flow. It has left out the question of how the interaction of the eddy field with the topography influences the mean flow in the basin. As has been noted in section 1, theoretical investigations predict a tendency towards a negative correlation between relative vorticity and topographic elevations with subsequent induction of a mean flow field. An inspection of the mean circulation in various regions of the subtropical model gyre indicated no changes in the thermocline; in the subthermocline levels, however, differences occurred between the solutions with and without topography. The main reason for not attempting an analysis of these effects here is that the grid size used in the present model seems not appropriate to adequately represent a correlation between topography and vorticity that is dominated by scales significantly smaller than the energetic scales (Holloway 1978). It is hoped that this issue can be elucidated by a model experiment, presently in progress, in which the resolution has been increased to ⅙°.

8. Conclusion

The introduction of a rough bottom topography in the eddy-resolving circulation model of C85 has a strong influence on the structure of the fluctuating flow field. The model is driven by steady wind and thermal forcing; eddies are generated by instability processes in the intense current region near the western boundary

and midlatitude jet (EKE > 1000 $cm^2 s^{-2}$), and in the westward flowing portion of the subtropical gyre ($\sim$80 $cm^2 s^{-2}$). In the instability regions, the thermocline eddy energy is not significantly affected by the bottom roughness; however, the topography reduces the radiation of energy away from those areas.

Stronger effects of the interaction with the rough floor appear in the deeper model levels. In the flat bottom case, the deep eddy energy reaches 20 $cm^2 s^{-2}$ in the interior of the subtropical gyre, considerably higher than observed in equivalent areas of the North Atlantic or North Pacific. The instantaneous flow shows a high vertical coherence with eddies of 200–300 km scale extending from the surface to the bottom. Deep eddy motions are scattered to smaller scales and effectively damped in the rough bottom case. Eddy energy below the thermocline does not exceed 5 $cm^2 s^{-2}$ in the gyre interior; the deep fluctuations show no coherence with the thermocline eddies. The change of the vertical structure of kinetic energy is more prominent in areas of weak flow intensity. In the flat bottom case the flow field becomes more barotropic away from the instability regions, which is opposite to the observed structure of the oceanic eddy field. The solution of the present model shows that topographic roughness can constitute an essential factor in the determination of the vertical eddy structure.

A zonally oriented, bandlike structure of the external mode constituted a striking feature of the flat bottom solution (C87), and was reflected in the strongly anisotropic particle dispersion in the subthermocline layers (Böning and Cox 1988). In the rough bottom case the barotropic bands as well as the anisotropic dispersion in the deep layers disappear while a preference of zonal motion remains characteristic of the low-frequency, thermocline flow. The particle behavior in the rough bottom case is more in accordance with the characteristics of SOFAR floats, which show an almost isotropic dispersion in the deeper layers.

Previous studies of stratified geostrophic turbulence were mostly based on the quasi-geostrophic approximation. A remarkable feature of the present primitive equation model is the longevity of thermocline eddies which keep their identity for more than a year. It is pointed out that the time and length scale of these intense vortices are indicative of intermediate–geostrophic rather than QG dynamics. The relevance of this result would have to be tested in experiments with higher horizontal resolution; the grid size of ⅓° used in the present study can only resolve the larger scales of the oceanic eddy field. The model solution derived here would suggest that the QG assumption, by neglecting the influence of vertical density advection, could miss an important factor in the dynamics of synoptic-scale ocean eddies.

Acknowledgments. I am deeply indebted to Kirk Bryan and Michael Cox whose continuous support and warm hospitality made working at GFDL and living in Princeton a pleasant experience. Helpful comments on the manuscript by G. Holloway, A. M. Treguier, G. Williams, and an anonymous reviewer are gratefully acknowledged. The GFD Program is sponsored by NOAA Grant NA84EAD00051.

REFERENCES

Anderson, D. L. T., and P. D. Killworth, 1977: Spin-up of a stratified ocean, with topography. *Deep-Sea Res.*, **24**, 709–732.

Barnier, B., 1986: A numerical study on the influence of the Mid-Atlantic Ridge on non-linear barotropic and first-mode baroclinic Rossby waves generated by seasonal winds. Tech. Rep., Mesoscale Air–Sea Interaction Group, Florida State University, Tallahassee.

Bell, T. H., 1975: Statistical features of sea-floor topography. *Deep-Sea Res.*, **22**, 883–892.

Böning, C. W., 1988: Characteristics of particle dispersion in the North Atlantic: An alternative interpretation of SOFAR float results. *Deep-Sea Res.*, **35**, 1379–1385.

——, and M. D. Cox, 1988: Particle dispersion and mixing of conservative properties in an eddy-resolving model. *J. Phys. Oceanogr.*, **18**, 320–338.

Bretherton, F. P., and D. B. Haidvogel, 1976: Two-dimensional turbulence above topography. *J. Fluid Mech.*, **78**(1), 129–154.

Bryan, K., 1969: A numerical method for the study of the circulation of the World Ocean. *J. Comput. Phys.*, **4**, 347–376.

Charney, J. G., and G. R. Flierl, 1981: Oceanic analogues of large scale atmospheric motions. *Evolution of Physical Oceanography*, B. A. Warren and C. Wunsch, Eds., MIT Press, 504–548.

Colin de Verdiere, A., 1983: Lagrangian eddy statistics from surface drifters in the eastern North Atlantic. *J. Mar. Res.*, **41**, 375–398.

Cox, M. D., 1985: An eddy resolving numerical model of the ventilated thermocline. *J. Phys. Oceanogr.*, **15**, 1312–1324.

——, 1987: An eddy resolving numerical model of the ventilated thermocline: Time dependence. *J. Phys. Oceanogr.* **17**, 1044–1056.

Dickson, R. R., 1983: Global summaries and intercomparison: Flow statistics from long-term current meter moorings. *Eddies in Marine Science*, A. R. Robinson, Ed., Springer-Verlag.

Freeland, H. J., P. Rhines, and H. T. Rossby, 1975: Statistical observations of trajectories of neutrally buoyant floats in the North Atlantic. *J. Mar. Res.*, **33**, 383–404.

Haidvogel, D. B., 1983: Periodic and regional models. *Eddies in Marine Science*, A. R. Robinson, Ed., Springer-Verlag.

Holland, W. R., 1973: Baroclinic and topographic influences on the transport in western boundary currents. *Geophys. Fluid Dyn.*, **4**, 187–210.

——, 1975: Energetics of baroclinic oceans. *Numerical Models of Ocean Circulation*, National Academy of Sciences, Washington, DC.

——, 1985: Simulation of mesoscale ocean variability in mid-latitude gyres. *Adv. Geophys.*, **28A**, 479–523.

——, and W. J. Schmitz, Jr., 1985: On the zonal penetration scale of model midlatitude jets. *J. Phys. Oceanogr.*, **15**, 1859–1875.

——, D. E. Harrison and A. J. Semtner, Jr., 1983: Eddy-resolving numerical models of large-scale ocean circulation. *Eddies in Marine Science*, A. R. Robinson, Ed., Springer-Verlag.

Holloway, G., 1986: Eddies, waves, circulation, and mixing: Statistical geofluid mechanics. *Annual Review of Fluid Mechanics*, **18**, 91–147.

——, 1978: A spectral theory of nonlinear barotropic motion above irregular topography. *J. Phys. Oceanogr.*, **8**, 414–427.

——, and M. Hendershott, 1974: The effect of bottom relief on barotropic eddy fields. MODE Hot Line News, No. 65.

Kampé de Fériet, J., 1939: Les fonctions aléatoires stationnaires et la théorie statistique de la turbulence homogène. *Ann. Soc. Sci. Bruxelles*, **59**, 145–194.

Krauss, W., and C. W. Böning, 1987: Lagrangian properties of eddy fields in the northern North Atlantic as deduced from satellite-tracked buoys. *J. Mar. Res.*, **45,** 259–291.

McWilliams, J. C., 1984: The emergence of isolated coherent vortices in turbulent flow. *J. Fluid Mech.*, **146,** 21–43.

Owens, W. B., and F. P. Bretherton, 1978: A numerical study of mid-ocean mesoscale eddies. *Deep-Sea Res.*, **25,** 1–14.

Rhines, P. B., 1977: The dynamics of unsteady currents. *The Sea,* Vol. 6, Wiley Interscience, 189–318.

——, 1979: Geostrophic turbulence. *Ann. Rev. Fluid Mech.*, **11,** 401–441.

——, and F. P. Bretherton, 1973: Topographic Rossby waves in a rough-bottomed ocean. *J. Fluid Mech.*, **61,** 583–607.

Richman, J. G., C. Wunsch and N. G. Hogg, 1977: Space and time scales of mesoscale motion in the western North Atlantic. *Rev. Geophys. Space Phys.*, **15,** 385–420.

Riser, S. C., and H. T. Rossby, 1983: Quasi-Lagrangian structure and variability of the subtropical western North Atlantic circulation. *J. Mar. Res.*, **41,** 127–162.

Robinson, A. R., Ed., 1983: *Eddies in Marine Science.* Springer-Verlag, 609 pp.

Rossby, H. T., S. C. Riser and A. J. Mariano 1983: The western North Atlantic—A Lagrangian viewpoint. *Eddies in Marine Science,* A. R. Robinson, Ed., Springer Verlag.

Schmitz, W. J., Jr., 1984: Abyssal eddy kinetic energy in the North Atlantic. *J. Mar. Res.*, **42,** 509–536.

——, and W. R. Holland, 1982: A preliminary comparison of selected numerical eddy-resolving general circulation experiments with observations. *J. Mar. Res.*, **40,** 75–117.

——, and ——, 1986: Observed and modeled mesoscale variability near the Gulf Stream and Kuroshio Extension. *J. Geophys. Res.*, **91,** 9624–9638.

——, —— and J. F. Price, 1983: Mid-latitude mesoscale variability. *Rev. Geophys. Space Phys.*, **21,** 1109–1119.

Treguier, A. M., and B. L. Hua, 1987: Influence of bottom topography on stratified quasi-geostrophic turbulence in the ocean. *Geophys. and Astrophys. Fluid Dyn.*, submitted.

Semtner, A. J., and W. R. Holland, 1978: Intercomparison of quasigeostrophic simulations of the western North Atlantic circulation with primitive equation results. *J. Phys. Oceanogr.*, **8,** 735–754.

Treguier, A. M., and B. L. Hua, 1987: Influence of bottom topography on stratified quasi-geostrophic turbulence in the ocean. *Geophys. and Astrophys. Fluid Dyn.*, submitted.

Verron, J., C. Leprovost and W. R. Holland, 1987: On the effects of a midocean ridge on the general circulation: Numerical simulations with an eddy-resolved ocean model. *J. Phys. Oceanogr.*, **17,** 301–312.

Williams, G. P., 1985: Jovian and comparative atmospheric modeling. *Adv. Geophys.*, **28A,** 382–429.

——, and T. Yamagata, 1984: Geostrophic regimes, intermediate solitary vortices and Jovian eddies. *J. Atmos. Res.*, **41,** 453–478.

——, and J. R. Wilson, 1988: The stability and genesis of Rossby vortices. *J. Atmos. Sci.*, **45,** 207–241.

Wunsch, C., 1981: Low-frequency variability in the sea. *Evolution of Physical Oceanography,* B. A. Warren and C. Wunsch, Eds., The MIT Press, 623 pp.

Yamagata, T., 1982: On nonlinear planetary waves: A class of solutions missed by the traditional quasi-geostrophic approximation. *J. Oceanogr. Soc. Japan,* **38,** 236–244.